AIScore − Chemically Diverse Empirical Scoring Function Employing Quantum Chemical Binding Energies of Hydrogen-Bonded Complexes

Stephan Raub,[†] Andreas Steffen,[‡] Andreas Kämper,[‡,§] and Christel M. Marian*[,†]

Institute of Theoretical and Computational Chemistry, Heinrich Heine University, Universitätsstrasse 1, D-40225 Düsseldorf, Germany, and Max Planck Institute for Informatics, Computational Biology and Applied Algorithmics; Stuhlsatzenhausweg 85, 66123 Saarbrücken, Germany

Received December 19, 2007

In this work we report on a novel scoring function that is based on the LUDI model and focuses on the prediction of binding affinities. AIScore extends the original FlexX scoring function using a chemically diverse set of hydrogen-bonded interactions derived from extensive quantum chemical *ab initio* calculations. Furthermore, we introduce an algorithmic extension for the treatment of multifurcated hydrogen bonds (XFurcate). Charged and resonance-assisted hydrogen bond energies and hydrophobic interactions as well as a scaling factor for implicit solvation were fitted to experimental data. To this end, we assembled a set of 101 protein−ligand complexes with known experimental binding affinities. Tightly bound water molecules in the active site were considered to be an integral part of the binding pocket. Compared to the original FlexX scoring function, AIScore significantly improves the prediction of the binding free energies of the complexes in their native crystal structures. In combination with XFurcate, AIScore yields a Pearson correlation coefficient of $R_P = 0.87$ on the training set. In a validation run on the PDBbind test set we achieved an R_P value of 0.46 for 799 attractively scored complexes, compared to a value of $R_P = 0.17$ and 739 bound complexes obtained with the FlexX original scoring function. The redocking capability of AIScore, on the other hand, does not fully reach the good performance of the original FlexX scoring function. This finding suggests that AIScore should rather be used for postscoring in combination with the standard FlexX incremental ligand construction scheme.

1. INTRODUCTION

Since the early 1980s, protein−ligand docking has evolved enormously.[1,2] Due to the importance of structure-based virtual screening methods in drug design, much effort has been spent on the development of efficient algorithms for generating binding geometries of protein−ligand complexes[3–6] and on the reliable assessment of their binding free energies by means of scoring functions. Docking tools usually generate a large set of proposals of binding geometries. Scoring functions are used to identify the binding geometry that corresponds most closely to the native binding mode. Furthermore, scoring functions are expected to predict the binding affinity. Preferably both criteria are fulfilled at the same time, i.e., the best ranked solution obtains a score that is close to the experimentally derived value. While the conformational search is often regarded as being resolved to a sufficient extent,[7] the prediction of binding affinities still remains a challenging field of research.[8,9]

Several types of scoring functions are used in current protein−ligand docking tools: empirical scoring functions that are based on experimental data by regression analysis,[10–14] empirical scoring functions that are derived from a knowledge base,[8,15–17] and force-field related scoring functions.[18–20] Recently, Raha and Merz[21] developed a scoring function based on semiempirical quantum mechanics which estimates electrostatic interactions and the solvation free energy during complexation. However, in a virtual screening setting this scoring function is currently not applicable due to its high computational demands.

The performance of an empirical scoring function highly depends on the quality of the database to which its parameters can be fitted. One of the major bottlenecks in its development is the availability of diverse and accurate experimental data. This problem can in principle be circumvented by augmenting experimental data by results of quantum chemical *ab initio* calculations which are independent from experimental results. Quantum chemical methods are widely used for detailed theoretical investigations of structural and energetic properties of chemical systems. Due to significant progress in method development and computer technology, the accuracy of *ab initio* data has more and more improved and comes close to the outcome of experimental techniques. However, accurate quantum chemical *ab initio* approaches must include electron correlation effects which are computationally expensive and can thus be applied to small model systems only.

Recently an extensive quantum chemical study of hydrogen-bonded complexes was carried out by some of us.[22] The major outcome was a chemically diverse system of donor and acceptor increments able to reproduce a wide range of the hydrogen bond interaction energies. Since hydrogen

* Corresponding author phone: +49-211-8113209; fax: +49-211-8113446; e-mail: Christel.Marian@uni-duesseldorf.de.
[†] Heinrich Heine University.
[‡] On leave from Max Planck Institute for Informatics.
[§] Present address: Wilhelm Schickard Institute for Computer Science, Division for Simulation of Biological Systems, University of Tübingen, Sand 14, 72076 Tübingen, Germany.

10.1021/ci7004669 CCC: $40.75
Published on Web 07/03/2008

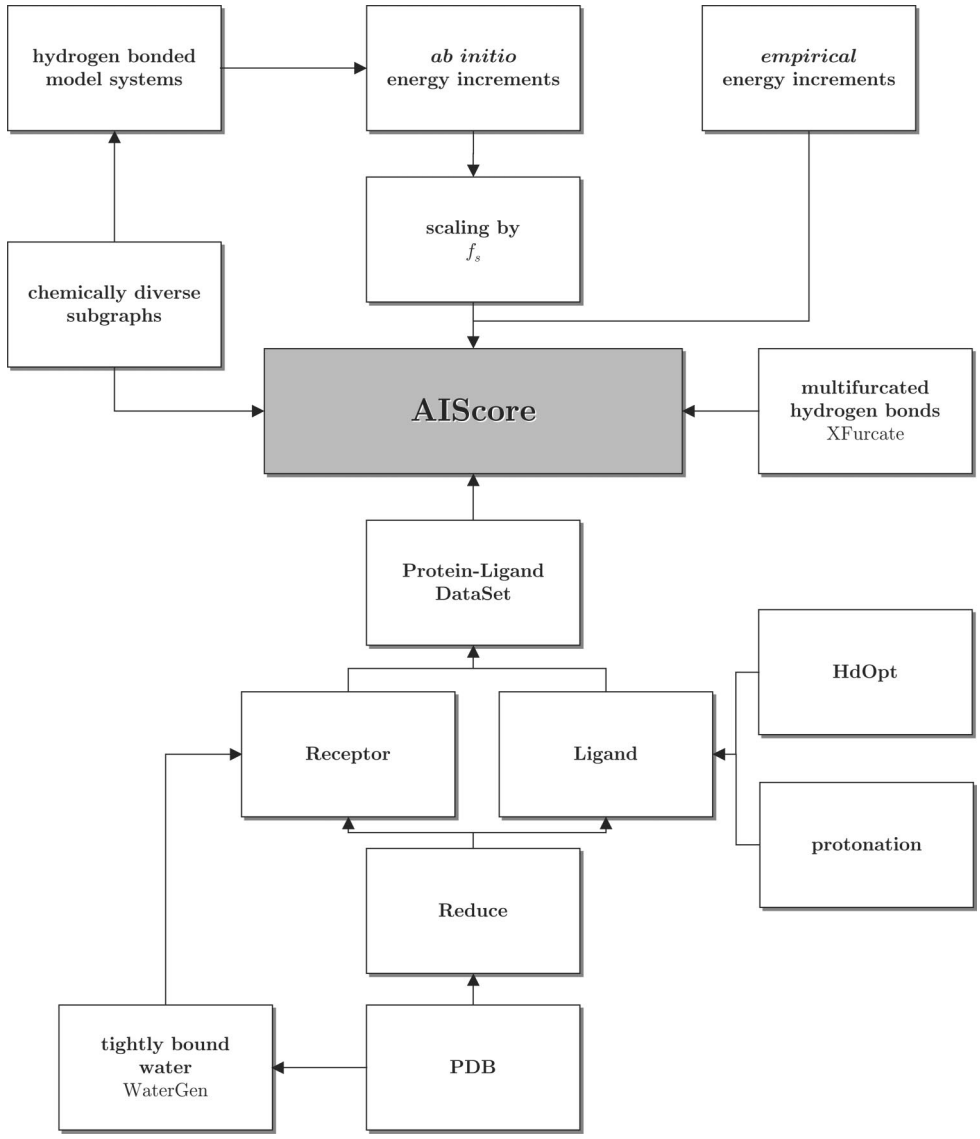

Figure 1. Schematic drawing of the design of AIScore.

bonds have a significant influence on chemical and biological systems, any computational tool that tries to predict interaction energies in such systems most likely fails if the variety of hydrogen bonds is not appropriately represented. A chemically reasonable handling of hydrogen bonds is thus a promising approach for improving protein−ligand scoring functions.

Here, we report on the development of a novel scoring function, called AIScore, which uses the results of these elaborate quantum chemical *ab initio* calculations to enhance the chemical diversity of the empirical scoring of the protein−ligand docking tool FlexX.[3]

2. METHODS

Our method is based on the LUDI interaction model[23,24] and the FlexX scoring function (FlexXScore)[3,10] which are briefly reviewed in Section 2.1.1. The original LUDI concept was enhanced with a description of multifurcated hydrogen bonds (Section 2.1.2). To represent the diversity of hydrogen bond donor and acceptor centers we developed a systematic tree of chemical subgraphs (see Section 2.1.3). Within our scheme, 19 types of hydrogen bond donors and 34 types of acceptors are implemented. Optimization schemes for parameters not derived from quantum chemical calculations are presented in Section 2.2.1. For the calibration of the interaction energy increments, we assembled a set of 101 protein−ligand complexes from the RCSB protein data bank (PDB)[25] with experimentally known binding affinities (Section 2.3). Sections 2.3.2 and 2.3.3 are devoted to the preparation of the binding pocket and the ligand prior to scoring. In this context, selection criteria are developed to decide which crystal water molecules are treated as part of the protein−ligand complex and which are discarded. Special attention has been spent on a chemically reasonable protonation of the ligand as well as the protein. Figure 1 illustrates the described design of AIScore.

2.1. The Scoring Function. *2.1.1. The Interaction Model.* The interaction models of FlexXScore and AIScore are derived from LUDI.[23,24] Herein, an interaction group consists of an interaction center and an interaction surface. Two interaction groups encounter a bonding situation if three conditions are fulfilled. First, only intermolecular interactions are taken into account. Second, the two interaction groups must possess compatible interaction types, e.g., one group

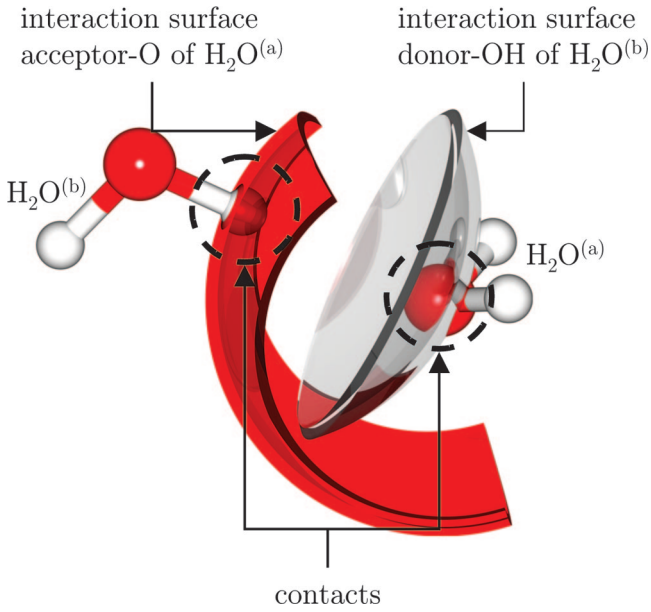

Figure 2. Interaction model of LUDI.

represents a hydrogen-bond donor and the other is a hydrogen-bond acceptor. Third, the interaction center of one group must lie on the interaction surface of the counter group and *vice versa* (Figure 2).

Each interaction group ω contributes an interaction energy increment ΔG_ω. The match score ΔG_{ia} is the sum of all involved increments ΔG_ω of a certain interaction type ia (with ia = hb (hydrogen bonds), aro (aromatic), or lipo (lipophilic)). The match score of the hydrogen bond in the water dimer in Figure 2, for example, is the sum of the acceptor increment of the sp^3 oxygen of the water molecule $H_2O^{(a)}$ and the donor increment of the hydrogen of $H_2O^{(b)}$. A penalty function $f(\Delta r, \Delta\alpha)$ penalizes deviations from ideal bond distances and angles.[12] The entire binding energy ΔG of a complex is calculated as the sum of all individual match scores ΔG_{ia} and the loss of entropy.[3]

$$\begin{aligned}\Delta G = \Delta G_0 + \Delta G_{rot} N_{rot} \\ + \Delta G_{hb} \sum_{H-bonds} f(\Delta r, \Delta\alpha) f_{chrg} \\ + \Delta G_{metal} \sum_{metal.int.} f(\Delta r, \Delta\alpha) f_{chrg} \\ + \Delta G_{aro} \sum_{arom.\ int.} f(\Delta r, \Delta\alpha) \\ + \Delta G_{lipo} \sum_{lipo.\ cont.} f_1(\Delta r) \\ + \Delta G_{ambig} \sum_{ambig.\ \ cont.} f_1(\Delta r) \\ + \Delta G_{clash} \sum_{clash\ \ cont.} f_2(\Delta r) \qquad (1)\end{aligned}$$

In the LUDI model, ΔG_0 and $\Delta G_{rot} N_{rot}$ describe the loss of entropy of the ligand as it is fixed within the binding pocket. Herein, ΔG_0 and ΔG_{rot} are constants and N_{rot} corresponds to the number of freely rotatable single bonds of the ligand. FlexX uses an extended form of the scoring function,[12] which was originally developed by Böhm.[10] Here ΔG_{hb}, $\Delta G_{metal.\ int.}$, and ΔG_{aro} represent the match scores of hydrogen bonds, metallic, and aromatic interactions, respectively. An additional scaling factor f_{chrg} of 1.667 is applied to every interaction increment whose interaction center carries a formal charge exceeding a defined threshold. The corresponding energy increments ΔG_ω were fitted to experimental binding energies in aqueous solution. All interaction types implemented in FlexX are listed in Table 1.

Table 1. Interactions and Parameterization of the Original and the Optimized FlexXScore

interaction	FlexXScore	FlexXScore(opt)
ΔG_ω hydrogen bond	−2.35	−0.37
ΔG_ω metallic	−2.35	−1.04
ΔG_ω aromatic/CH	−0.35	−0.35
ΔG_0	+5.40	−10.59
$\Delta G_{lipo/ambig}$	−0.17	−0.33

Table 2. Representative Results of a Quantum Chemical *ab Initio* Study of H-Bonded Complexes with Oxygen as Acceptor and Donor according to Ref 22[b]

complex	don.	acc.	$\Delta E^{CPC}{}_{MP2}$	d_{H-B}
$H_2O\cdots H_2O$	O.3H	O.3	−20.38	1.86
$H_2O\cdots$m-butinol[a]	O.3H	O.3	−13.04	2.00
$H_2O\cdots$MeCOOH	O.3H	O.3	−17.47	1.97
ethenol$\cdots$EtOH	O.3H	O.3	−34.44	1.77
PhOH$\cdots$EtOH	O.3H	O.3	−36.71	1.80

[a] 3,3-Dimethylbut-1-yn-1-ol. [b] The binding energy ΔE [kJ mol^{-1}] was determined by second-order Møller−Plesset perturbation theory including counterpoise corrections. d_{H-B} [Å] denotes the hydrogen bond length.

The last three terms ΔG_{lipo}, ΔG_{ambig}, and ΔG_{clash} score the atom-atom contacts between receptor and ligand. ΔG_{lipo} considers only pairs of nonpolar atoms, and ΔG_{ambig} considers pairs of one polar and one nonpolar atom. ΔG_{clash} penalizes overlaps of protein and ligand.

In the original FlexXScore, the interaction energy increments ΔG_ω are identical for all neutral oxygen and nitrogen hydrogen bond donors and acceptors (ΔG_ω = −2.35 kJ mol^{-1}), irrespective of their chemical contexts. Quantum chemically determined *ab initio* interaction energies of hydrogen-bonded complexes, on the other hand, extend over a wide range.[26−28] In a series of isolated complexes containing an sp^3 oxygen hydrogen bond donor and an sp^2 oxygen hydrogen bond acceptor, for instance, the interaction energies approximately span a range from −13 kJ mol^{-1} to −37 kJ mol^{-1} (Table 2). [It should be noted that these values do not include solvent effects and are therefore not directly comparable to the FlexXScore value of ΔG_ω = −2.35 kJ mol^{-1}.] Moreover, some of us showed recently[22] that sulfur in sulfides, disulfides, and thiols can be a hydrogen bond acceptor of remarkable strength. This fact is not accounted for in the original scoring scheme of FlexXScore, in which sulfur is presently treated as a hydrophobic interaction center only.

2.1.2. Multifurcated Hydrogen Bonds. Multiple hydrogen bonds that share one acceptor atom were introduced in 1939 by Albrecht and Corey.[29] The authors proposed a *bifurcated bond* (see **1** in Figure 3) to explain the crystal structure of α-glycine. Later, the terminus *bifurcated hydrogen bond* was also used for other binding situations (see **2** and **3** in Figure 3) which can be found, for instance, in specific water dimers or trimers.[30] Today, bifurcated hydrogen bonds are used to explain many biological structures and their comprised interactions.

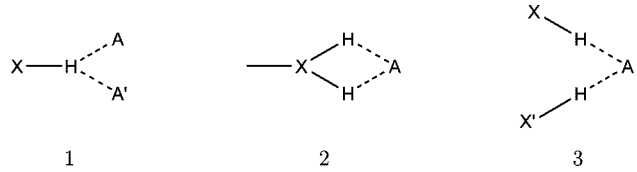

Figure 3. Types of bifurcated hydrogen bonds.

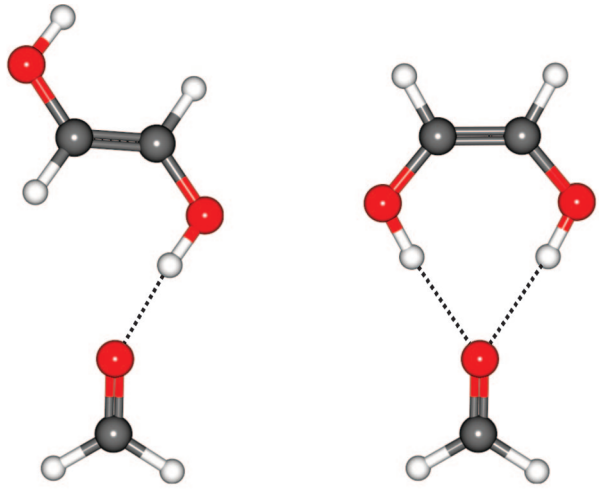

Figure 4. MP2 interaction energies of formaldehyde complexed with *trans*-1,2-ethenediol (*left*) and *cis*-1,2-ethenediol (*right*).

In the original LUDI model, these types of hydrogen bonds are not differentiated from standard hydrogen bonds. To illustrate the relevance of a special treatment of bifurcated hydrogen bonds, we carried out quantum chemical *ab initio* calculations on two model systems using the same methods and basis sets as described in ref 22. A comparison of the results for formaldehyde, complexed with either the *trans* form of 1,2-ethenediol (single hydrogen bond, Figure 4 *left*) or the *cis* form (bifurcated hydrogen bond of type **3**, Figure 4 *right*), shows that a bifurcated hydrogen bond yields significantly less binding energy than two separate hydrogen bonds. Thus, protein−ligand complexes with many bi- or multifurcated hydrogen bonds are unreasonably overscored in the original FlexXScore scheme (see Section 3). In addition to the overbinding effect, the undifferentiated scoring of these hydrogen bonds may have a structural influence during the incremental construction procedure as partial placements with multifurcated hydrogen bonds are favored.

To include multifurcated hydrogen bonds in the FlexX-Score scoring function, we assume that each interaction group contributes its energy increment ΔG_ω only once, irrespective of the number of contacts it forms out. A schematic illustration of this model for a bifurcated hydrogen bond (XFurcate) in comparison with the original FlexXScore scoring scheme is shown in Figure 5. In this specific example, the hydrogen bond donor increments are treated equally in both scoring schemes. Conversely, the sp^2 oxygen acceptor shares its energy increment between the two hydrogen bonds in the XFurcate model, whereas it contributes its full score in the FlexX scheme. The XFurcate model is easily extended to multifurcated hydrogen bonds: An interaction group with n contacts contributes $\Delta G_\omega/n$ to each contact.

2.1.3. Chemically Diverse Molecular Subgraphs. FlexX uses a library of predefined molecular fragments and their

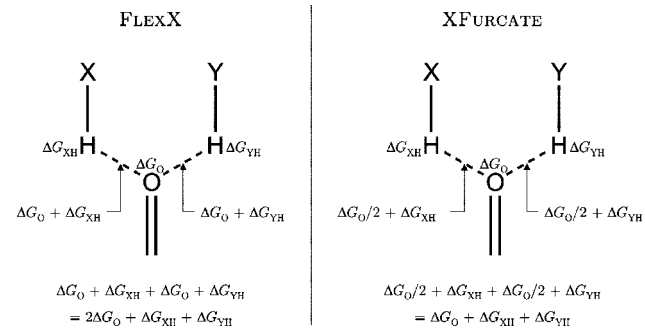

Figure 5. Schematic illustration of the difference in scoring bifurcated hydrogen bonds. ΔG_O is the energy increment for the sp^2-oxygen acceptor, and ΔG_{XH} and ΔG_{YH} are the hydrogen-bond donor increments of X−H and Y−H.

interactions. These molecular fragments are represented as molecular subgraphs, in which a node represents an atom of a given type and an edge represents a covalent bond. Atom and bond types are defined by their Sybyl notation.[58] When processing a ligand, FlexX assigns the interactions by matching the molecular subgraphs from the database with the graph representation of the ligand. Only atom types, bond types, and the corresponding connectivity are matched; geometric properties are totally ignored.

In this work, we introduce a systematic approach to describe different chemical contexts of an interaction center by means of chemical subgraph trees. These subgraph trees are constructed in the following way: Starting from the typical hybridization states of oxygen, nitrogen, and sulfur, respectively, we add biochemically relevant atom types that can form a meaningful chemical bond. This is the first level of subgraphs. The second level is generated by adding all reasonable atom types to the atoms of the first level, etc. The subgraph trees of hydrogen bond donors and acceptors employed in AIScore are shown explicitly in the Supporting Information. The maximum level depth occurring in this scheme is four. In this way a treelike system of molecular subgraphs develops, the complexity of which increases with each level. Every element of the subgraph tree obtains a priority that corresponds to its level depth. In this way, a specific molecular subgraph, such as an amidic sp^2 oxygen that is found on level 4, obtains a high priority (4) while a more general term, such as an sp^2 oxygen attached to a carbon atom, receives a low priority (2).

When analyzing binding sites of a receptor−ligand complex, an interaction term is assigned to any functional group that corresponds to the subgraph with the highest priority. If a functional group is encountered which is not represented by a specific entry in the subgraph tree, the more generic subgraph of the next lower level is taken, etc.

Figure 6 exemplifies the interaction-type assignments according to the original FlexXScore and the novel AIScore schemes. In this hypothetical molecule, two sp^2 oxygen and two sp^3 oxygen atoms occur which are scored alike in FlexXScore, whereas they are differentiated as sp^2 amidic oxygen, ester sp^2 oxygen, ether sp^3 oxygen, and ester sp^3 oxygen hydrogen bond acceptor in AIScore. The sp^3 sulfur atom is considered a hydrophobic interaction center in the FlexXScore scoring scheme, whereas it acts as a hydrogen bond acceptor in AIScore. Finally, the sp^3 nitrogen hydrogen bond donor is recognized as part of an amide group in AIScore. This example illustrates

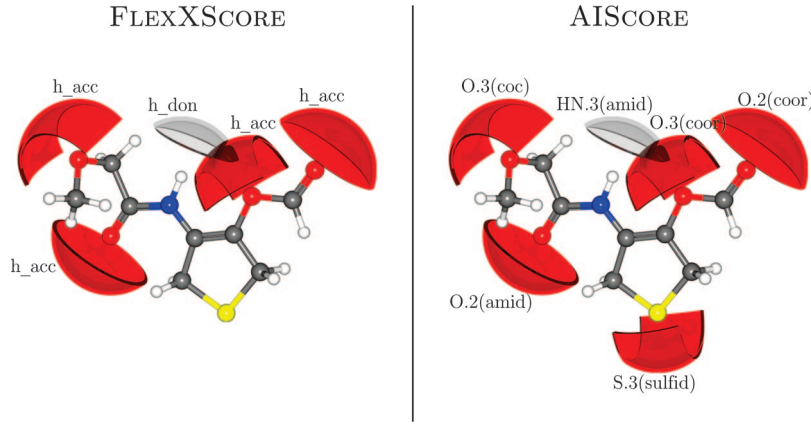

Figure 6. Comparison of the interaction surfaces assigned to this hypothetic molecule by FlexXScore and AIScore.

the increased chemical diversity of interaction types in our extended scoring scheme.

2.2. Parameterization. *2.2.1. Parameter Optimization Protocol.* The following protocol was chosen for the optimization of parameters: Our software scores the ligand in its native position. All complexes i are scored in one run, and the root-mean-square error between the scored energies and experimental binding affinities of a calibration set (RMSE) is calculated.

$$RMSE = \sqrt{\frac{\sum_{i}^{n} (\Delta G_{scored}(i) - \Delta G_{exp.}(i))^2}{n}} \qquad (2)$$

Because of their different orders-of-magnitude, we used different search intervals for increments ΔG_ω and ΔG_0 (-10.0, $+5.0$ kJ mol^{-1}), the scaling factor f_s (0.0, 0.2), and the contact score $\Delta G_{lipo/ambig}$ (-0.4, 0.0 kJ mol^{-1}). The search ranges were partitioned into 300 equidistant intervals. The optimization procedure commenced with the generation of 1000 random 15 dimensional starting vectors. With each of these starting vectors we performed an iterative grid search in the following way: Successively, each parameter i is scanned while holding all others frozen to their current values. If a new minimum along this path is found, the parameter i is set to the corresponding value, otherwise it is left unchanged. After the 15th one-dimensional scan we check whether at least one parameter i has changed. In this case, the procedure is started all over again. Afterward we refined the outcome of this grid search with a continuous downhill algorithm without any restriction in stepsize or range.

2.2.2. AIScore Parameters. The functional form of AIScore is given by

$$\begin{aligned} \Delta G = \Delta G_0 &+ \Delta G_{rot} N_{rot} \\ &+ \sum_{don}^{N_d} \sum_{acc}^{N_a} \delta_{match} (\Delta G_\omega(don) \\ &+ \Delta G_\omega(acc)) f(\Delta r, \Delta\alpha) \\ &+ \Delta G_{lipo/ambig} \sum_{lipo/ambig\ cont.} f_1(\Delta r) \\ &+ \Delta G_{clash} \sum_{clash\ cont.} f_2(\Delta r) \end{aligned} \qquad (3)$$

where N_d and N_a are the number of donors and acceptors, respectively. δ_{match} equals to one if the corresponding donor and acceptor form a matched contact and is equal to zero otherwise. Please notice that the increments ΔG_ω depend not only on the type of interaction (i.e., hydrogen bonds, metallic interactions, etc.) but also on the particular functional group. For the increments

$$\Delta G_\omega = \begin{cases} \Delta G_\omega^{QC} = f_s \Delta E_\omega^{QC} & \text{quantum chemically} \\ & \text{derived increment exists} \\ \Delta G_\omega^{fitted} & \text{otherwise} \end{cases} \qquad (4)$$

For AIScore 15 parameters (see Table 3) were fitted to experiment while keeping the ratios of the energy increments describing neutral hydrogen bonds fixed to the values derived from recent quantum chemical *ab initio* calculations.[22] Interactions of carbon centers forming CH acidic hydrogen bonds with a strong hydrogen bond acceptor were disregarded. Only the ΔG_{rot} term and the penalty for an atom clash were left unchanged with respect to the original version of FlexXScore. Since we use particular interaction terms for charged interaction centers, the scaling factor f_{chrg} for charged interactions is always set to 1. In contrast to the original FlexX protocol, also interactions other than atom clashes are allowed to have positive energies, i.e., their contributions to the total score are not set to zero.

Solvent Effect on Neutral Hydrogen Bonds. Quantum chemically determined binding energies of isolated hydrogen-bonded complexes cannot be employed directly for defining the match score of a given interaction between a ligand and a protein. In reality both, the protein and the ligand, are embedded in a solvation shell of water molecules and have to be (partially) desolvated before the protein−ligand complex can be formed. The energy required for the latter process typically leads to a decrease of the total complex binding energy. Here, we assume that for a given solvent this decrease scales linearly with the hydrogen bond strength of an interaction group. With this assumption we can model the solvent effect on the interaction energies of 19 types of hydrogen bond donors and 34 types of hydrogen bond acceptors by means of a single factor f_s that scales the *in vacuo* increments. Hence, the interaction energy increment of a donor or an acceptor ΔG_ω^{QC} is given as

$$\Delta G_\omega^{QC} = f_s \Delta E_\omega^{QC} \qquad (5)$$

where ΔE_ω^{QC} is the energy increment calculated by quantum chemical methods *in vacuo*. In order to predict binding affinities in close agreement with experimental results, the

Table 3. Freely Optimized Parameters of AIScore and FlexXScore(aug) and their Frequency in the Training Set ($f_{training}$) and in the PDBbind Set ($f_{PDBbind}$)

parameter name	description	AIScore	FlexXScore(aug)	$f_{training}$	$f_{PDBbind}$
Scaling					
f_s	factor for scaling down the *ab initio* increments	0.16			
ΔG_ω HB	score of general neutral hydrogen bonds		−2.37		
Special Hydrogen Bonds					
ΔG_ω O.2(peptide)	sp^2 acceptor O of the peptide backbone	−1.58	+0.16	175	1384
ΔG_ω O.2(po_so)	partially charged sp^2 O connected to P or S	−4.20	−3.56	12	87
ΔG_ω HN.3(peptide)	H-donor at the amid N of the peptide backbone	+0.55	+0.54	119	1004
Ionic Interactions					
ΔG_ω O.co2(coo-)	negatively charged O of carboxylate groups	−1.82	−0.78	183	1257
ΔG_ω O.co2(po)	negatively charged O connected to a P	−0.98	−0.01	39	640
ΔG_ω HN+(cmn)	H on a positively charged N	+3.83	+2.82	81	772
ΔG_ω HN+(ARG)	positively charged H-donor of arginine	−0.61	−0.13	58	543
Metallic Interactions					
ΔG_ω metal_chrg	a negatively charged atom binding to a metal	−9.38	−20.77	3	0
ΔG_ω metal_d	transition metal ion	−5.91	−5.90	14	146
ΔG_ω metal_s	alkali metal and alkaline earth metal ions	−5.39	−9.67	6	62
Lipophilic Interactions					
ΔG_ω CH	CH-group of any hybridization	−0.05	+0.18	446	2325
ΔG_ω aro	π-system of an aromatic ring	−0.51	−0.75	114	1133
Global Parameters					
ΔG_0		−5.74	−6.94		
$\Delta G_{lipo/ambig}$		−0.31	−0.31		

factor f_s is fitted to experimental binding affinities.

Resonance-Assisted Hydrogen Bonds. The binding energies of strong hydrogen bonds in conjugated molecular systems are characterized by resonance-enhanced electrostatic interactions and charge polarization (occurring in DNA bases, for instance). The additive donor and acceptor increments derived in ref 22 systematically underestimate the quantum chemical *ab initio* binding energies by about 30%. For this reason and because of the importance of these hydrogen bonds in biological systems, the energy increment of an HN.3 donor in pyrimidine and purine rings of DNA bases was set to 1.3 times the increment of a simple planar HN.3 group. The energy increments of peptides and partially charged O.2 acceptors in phosphates and sulfates (see Table 3) were fitted to experiment.

Salt Bridges. Interaction energies of salt bridges cannot be evaluated by quantum chemical methods *in vacuo* because zwitterions are not stable in the absence of a polar solvent. Therefore, the match scores of four types of ionic interactions (see Table 3) were freely adjusted to experimental binding energies, too.

Metal−Ligand Interactions. In principle, metal−ligand interactions are accessible to quantum chemical *ab initio* methods.[31–33] However, metal atoms and ions tend to form complexes with multiple ligand groups at the same time, and the partition of the total energy is not obvious. Furthermore, they are not frequently represented in our training data set. We have therefore refrained from generating a separate *ab initio* database for metal−ligand interactions here.

Lipophilic Interactions. These interactions are considerably weaker than hydrogen bonds and ionic interactions. They originate mainly from entropic effects due to exclusion from the solvent cage. To calculate these effects in an *ab initio* manner requires explicit inclusion of the solvent and conformational averaging which is out of reach with present day computer resources. Despite their weakness, lipophilic interactions cannot be neglected since they are highly abundant in biological systems. In addition to the entropic contributions (see next paragraph) dispersion forces play a significant role in lipophilic interactions. Due to change of hydrogen-bond strengths in AIScore with respect to FlexXScore, the increments of aliphatic and aromatic interaction groups had to be readjusted to match experimental binding energies.

Entropic Contributions and Pauli Repulsion. It turned out that the parameters of AIScore were very sensitive to the factors with which all pairs of atom contacts are scaled, depending on their mutual distance. While we left the clash score parameter for close contacts unchanged, the parameters for attractive contacts between two hydrophobic atoms and the so-called ambiguous contacts between a hydrophobic center on one side and a hydrophilic center on the other side were optimized with the constraint that both remain equal. It should be mentioned that the increments of aliphatic and aromatic interaction groups and the parameter $\Delta G_{lipo/ambig}$ are highly correlated. Small absolute values of the latter lead to large increments ΔG_{CH} and ΔG_{aro} (see Table 3) and *vice versa*. However, we did not find an easy way to eliminate one or the other parameter. In addition, the ΔG_0 term of eq 1 was readjusted.

2.2.3. Adjusted FlexXScore Parameters. To assess the performance of our diverse subgraph scheme in comparison to the original FlexX scoring scheme, we furthermore carried out a similar optimization protocol as described above for two other scoring functions.

In the first scenario, FlexXScore(opt), 5 parameters, i.e., ΔG_0, the parameter for the attractive atom contacts ($\Delta G_{lipo} = \Delta G_{ambig}$), and the energy increments of the interactions were reoptimized in a least-squares fit of the experimental binding affinities.

In a second setup, named FlexXScore(aug), all empirical interaction parameters of AIScore were fitted to experimental data. Instead of f_s, here the score HB of all normal hydrogen bonds is optimized. FlexXScore(aug) has the same number of degrees of freedom as AIScore. The only difference between the two schemes is the higher chemical diversity of neutral hydrogen bonds.

2.3. Data Set of Protein−Ligand Complexes. *2.3.1.*

Selection of the Calibration Set. For the parameter optimization and evaluation of our scoring schemes, we are essentially depending on trustful experimental data, the presence of structurally conserved water molecules, and additionally—due to our chemically diverse subgraph scheme—on a representative set of diverse interaction types. We based our selection on protein−ligand complexes used in other scoring function parametrization papers,[11,13,21,36] taking into account only those 101 complexes which fullfil the following criteria:

- well-defined binding mode of the ligand
- no large conformational changes of the protein upon ligand binding
- assured binding affinity (from original literature[35,37–46] if available)
- when it is known that tightly bound water molecules mediate interactions, these waters should be resolved in the crystal structure
- the biological molecule is identical with the asymmetric unit of the crystal structure

Within this set of complexes (Table 4), chemically diverse ligands (alcohols, ketones, phosphates, sulfates, amines, sulfonamides, carbonic acids, sugars, heterocycles, nucleobases, peptides, urea derivatives, etc.) and pharmacologically relevant classes of proteins (hydrolases, oxidoreductases, transferases, protein kinases, lyases, proteinases, ligases, HIV-1 proteases, immunoglobulins, thrombins, several binding proteins, transport proteins, etc.) are present.

2.3.2. Preparation of the Binding Pocket. The most probable protonation states of the protein−ligand binding sites in the training set were assigned using Reduce version 3.03.[48] To generate the receptor descriptor file (RDF) required for FlexX, we used RDFWizard, a fully automated in-house script. RDFWizard reads the output of Reduce as well as the reference coordinates of the ligand and identifies the residues in the vicinity of the ligand, including hetero groups. Subsequently, the protonation state for each of the amino acids is identified, and the corresponding amino acid template (e.g., histidine protonated at N_ε) is assigned. Finally, the torsion angles of all hydroxyl and thiol groups are identified. All results are written to the RDF. Metal hetero groups are automatically included, and nonmetal hetero groups are manually added, if necessary.

Typically, protein crystals contain up to 70% water.[49,50] In experimental crystal structure studies, numerous examples of water-mediated protein−ligand interactions have been reported.[51–53] Here, the placement of the ligand can be sterically or electrostatically unfavorable if a mediating water molecule is disregarded. In these cases a water molecule has to be considered as a part of the active site as it significantly modifies the structure and the properties of the binding pocket. A typical example for the participation of a strongly interacting water molecule is the tightly bound water molecule in center of HIV-1 protease.[39]

Unfortunately, hydrogen positions of water molecules are not resolved within most crystal structures. In the first step we added hydrogens to all water molecules within a 3.5 Å sphere around the ligand. The positions of these hydrogens were optimized by means of the MMFF94 force field[54] in the presence of the ligand (in the orientation found in the complex) and the binding site. Afterward it was checked whether the added water molecules affect the positions of donor hydrogens of the ligand. In none of our complexes this was the case.

In order to decide whether a water molecule should be considered as part of the binding pocket or be removed, we used a protocol which is in some respects similar to Waterscore.[51] We defined a water molecule as part of the active site, if three criteria are fulfilled: (*i*) the water molecule must be bound to the active site via one or more hydrogen bonds, (*ii*) the water molecule needs to form at least one hydrogen bond with the ligand, and (*iii*) the water molecule should be sufficiently immobile within the active site.

These criteria were quantified in the following way. (*i*) A water molecule is discarded, if its interaction with the binding pocket $\Delta G > -4.1$ kJ mol^{-1}. (*ii*) Water molecules that pass criterion (*i*) are assessed by scoring their hydrogen bonds to the ligand. A water molecule with a ligand binding free energy $\Delta G < -3.1$ kJ mol^{-1} is incorporated into the active site if (*iii*) the oscillation of its oxygen atom around the position specified in the crystal structure data is small. The latter condition is considered to be fulfilled, if the isotropic temperature factor of the oxygen atom $B_O < 30$ Å^2.

2.3.3. Ligand Protonation and Assignment of Atom Types. The coordinates of non-hydrogen atoms of the ligands were directly taken from the Reduce-optimized PDB file. We used CORINA[55] to assign Sybyl atom types and to protonate the molecules where protons had not been added by Reduce. All type assignments and protonation states were manually inspected and, if necessary, changed as demonstrated in the following example.

Figure 7 shows a schematic representation of the ligand and the interacting amino acids of PDB entry 8ABP. In the upper part the dihedral angles of the protons of the sugar are those as calculated by CORINA. With this configuration four hydrogen bonds to three amino acids can be established. By changing only the dihedral angles of three protons with the method proposed, seven hydrogen bonds can be established to five amino acids (lower part of Figure 7).

If a hetero group is present in the data bank of the Reduce program, the positions of hydrogen atoms connected to this group were optimized with this program. Otherwise, hydrogen atoms bound to ligand oxygen or sulfur atoms that are involved in hydrogen bonding to the active site were optimized using a two-step procedure HdOpt which is part of the tool FlexR.[56,57] In the first step, starting positions for each individual hydroxyl and thiol hydrogen were identified by rotating the H−O or H−S bonds about the HO-R and HS-R axes. Here, the step-size was set to 15 degrees. For each position the interaction energy with the protein was calculated using the Tripos force field.[58] The position yielding the most favorable interaction energy was retained. In the second step, all coordinates of polar hydrogen atoms of the ligand were simultaneously optimized in the presence of the active site. In this step we used a quasi-Newton minimization technique. Optimized hydrogen positions were used for all subsequent procedures.

2.4. Assessment. For qualitatively assessing the performance of our scoring function, the Pearson correlation coefficient (R_P), the standard deviation (*SD*), and the unsigned mean error (*ME*) were chosen to be in line with other evalutations of scoring functions.[59,60] When x denotes the experimental binding energies, y denotes the scores, and

Table 4. Complexes of Data Set

PDB code	protein	ligand	ΔG_{exp} [kJ mol^{-1}]	hetero groups	ref
1A1C	SH2 of c-src tyrosine kinase	MCP-PTR	−36.51		ref 47
1A42	carbonic anhydrase II	brinzolamide	−56.42	Zn	ref 44
1A4W	alpha-thrombin	5-(dimethylamino)-1-naphthalenesulfonic acid-2-ethylpiperidine-2-ketothiazole	−33.77	HOH031, Na	ref 47
1AAQ	HIV-1 protease	hydroxyethylene isostere	−47.92	HOH001	ref 47
1ABF	L-arabinose-binding protein	D-fucose	−30.92		ref 47
1ACJ	acetylcholinesterase	tacrine	−41.65		ref 47
1ADD	adenosine deaminase	1-deaza-adenosine	−38.45	Zn	ref 36
1AJ7	immunoglobulin 48g7 fab	5-(para-nitrophenyl phosphonate)-pentanoic acid	−22.08		ref 37
1ATL	atrolysin c	2-(thiomethylene)-4-methylpentanoic acid	−35.83	Zn	ref 47
1AVN	carbonic anhydrase II	histamine	−22.25		ref 47
1AX2	lectin	N-acetyllactosamine	−22.70	Ca, Mn	ref 35
1B1H	oligo-peptide binding protein	homophenylalanine	−40.11	HOH071	ref 47
1B2H	oligo-peptide binding protein	ornithine	−25.90		ref 47
1B3F	oligo-peptide binding protein	LYS-HIS-LYS	−39.31	HOH018	ref 47
1BAP	L-arabinose-binding protein (P254G)	L-arabinose	−39.08		ref 47
1BCU	alpha-thrombin	proavin	−28.53		ref 47
1BDQ	HIV-1 protease (T31S, V32I, L33V, E34A, E35G, M36I, S37E, I47V, V82I)	SB203386	−39.71		ref 47
1BDR	HIV-1 protease (T31S, L33V, E34T, E35G, M36I, S37E)	SB203386	−44.35		ref 21
1BHX	alpha-thrombin	SDZ 229−357	−39.02		ref 47
1BN1	carbonic anhydrase II	AI5917	−53.29		ref 44
1BN4	carbonic anhydrase II	N-[(4-methoxyphenyl)methyl]2,5-thiophenedesulfonamide	−53.12	Zn	ref 44
1BQP	pea lectin	D-mannopyranose	−16.60	Ca, Mn	ref 35
1BRA	trypsin (D189G, G226D)	benzamidine	−10.38		ref 47
1C1R	trypsin	(5-amidino-2-benzimidazolyl) (2-benzimidazolyl)methane	−43.53	Mg, Zn	ref 47
1CAQ	stromelysin-1	diphenyl piperidine sulfonamide	−44.04	Ca, Zn	ref 47
1CPS	carboxypeptidase A	[L-(-)-2-carbpoxy-3-phenylpropyl]methylsulfodiimine	−38.00	Zn	ref 34
1D09	aspartate transcarbamoylase	N-(phosphonacetyl)-L-aspartic acid	−43.19		ref 47
1D7H	FK506-binding protein	DMSO	−9.83		ref 21
1D7I	FK506-binding protein	DSS	−20.54		ref 47
1D7J	FK506-binding protein	4-hydroxy-2-butanone	−18.83		ref 47
1DD7	inducible nitric oxide synthase	1PM	−49.39	heme	ref 38
1DI8	cyclin-dependent protein kinase 2	DTQ	−34.69		ref 21
1DL7	antibody m3c65	p-nitrophenyl-phosphocholine	−32.17		ref 45
1DMP	HIV-1 protease	DMP450 of Dupont-Merck	−54.48		ref 47
1DWD	alpha-thrombin	NAPAP	−46.67		ref 34
1E1V	cyclin-dependent protein kinase 2	NU2058	−28.07		ref 47
1E1X	cyclin-dependent protein kinase 2	NU6027	−34.04		ref 47
1EJN	urokinase-type plasminogen activator	N-(1-adamantyl)-N′-(4-guanidinobenzyl)urea	−32.06		ref 47
1ERB	retinol binding protein	N-ethyl retinamide	−40.22		ref 47
1FEL	retinol binding protein	feretinide	−38.48		ref 21
1FKB	FK506-binding protein	rapamycin	−55.34		ref 47
1FKF	FK506-binding protein	FK506	−53.63		ref 47
1FKG	FK506 binding protein	rotamase inhibitor	−45.64		ref 47
1GCZ	macrophage migration inhibitory factor	7-hydroxy-2-oxochromene-3-carboxylic acid ethyl ester	−29.27		ref 47
1GHY	thrombin	2-(3-hydroxy-pyridin-2-yl)-1H-benzoimidazole-5-carboxamidine	−46.21	Na, Zn	ref 47
1GIH	cell division protein kinase 2	CDK4 inhibitor 1	−40.59		ref 21
1HBV	HIV-1 protease	SB202127	−36.34	HOH501	ref 47
1HIH	HIV-1 protease	CGP 53820	−45.93	HOH006	ref 47
1HPV	HIV-1 protease	VX-478	−52.60	HOH201	ref 47
1HPX	HIV-1 protease	KNI-272	−53.06	HOH301, HOH608	ref 47

Table 4. Continued

PDB code	protein	ligand	ΔG_{exp} [kJ mol^{-1}]	hetero groups	ref
1HSG	HIV-1 protease	indinavir L-735,524	−53.74	HOH308	ref 47
1HVI	HIV-1 protease	A77003 (R,S)	−57.48	HOH415	ref 39
1HVJ	HIV-1 protease	A78791 (S,-)	−59.65	HOH415	ref 39
1HVK	HIV-1 protease	A76928 (S,S)	−57.70	HOH415	ref 39
1HVL	HIV-1 protease	A76889 (R,R)	−51.35	HOH415	ref 39
1HVR	HIV-1 protease	XK263 of Dupont-Merck	−54.26		ref 47
1L8B	eukaryotic translation initiation factor 4e	7-methyl-guanosine-5′-triphosphate	−39.08	HOH036	ref 47
1MES	HIV-1 protease (I84V)	DMP323	−43.93		ref 47
1MEU	HIV-1 protease (V82F, I84V)	DMP323	−34.80		ref 47
1MSM	HIV-1 protease	KNI-764	−59.79	HOH001	ref 46
1NNB	neuraminidase	DANA	−30.24	Ca	ref 34
1ONA	concanavalin A	MAN-MMA-MAN	−30.96	Ca, Mn	ref 35
1ORK	tetracycline repressor	9-(N,N-dimethylglycylamido)-6-demethyl-6-deoxytetracycline	−50.26	Mg	ref 47
1PPH	trypsin	3-TAPAP	−33.77		ref 40
1PPM	penicillopepsin	phosphoanalog 2	−33.09		ref 47
1RBP	plasma retinol-binding protein precursor	retinol	−38.34		ref 36
1RDI	mannose-binding protein	alpha-L-methyl-fucose	−11.75	Ca	ref 47
1RDJ	mannose-binding protein	beta-L-methyl-fucose	−9.47	Ca	ref 47
1TMT	alpha-thrombin	CGP 50,856	−35.60		ref 47
1TNJ	trypsin	2-phenyl-ethylamine	−11.18		ref 47
1TNK	trypsin	3-phenyl-propylamine	−8.50		ref 47
1TNL	trypsin	tranylcypromine	−10.73		ref 47
1ULB	purine nucleoside phosphorylase	guanine	−25.11		ref 34
1YDR	cAMP-dependent protein kinase	H7 protein kinase inhibitor	−31.49		ref 47
2BZA	trypsin	benzylamine	−15.97	SO4	ref 47
2CTC	carboxypeptidase A	L-phenyl lactate	−22.19	Zn	ref 34
2PHH	p-hydroxybenzoate hydroxylase	p-hydroxy-benzolate	−26.70		ref 36
2QWC	neuraminidase (R292K)	neu5ac2en	−20.25	HOH121G, Ca	ref 47
2QWD	neuraminidase (R292K)	4-amino-neu5ac2en	−27.67	HOH121G, Ca	ref 47
2TSC	thymidylate synthase	CB3717	−48.61		ref 36
2WEA	penicillopepsin	MCP1P31a	−35.23		ref 21
2YPI	triosephosphate isomerase	2-phospho-glycolate	−27.50		ref 47
3AID	HIV-1 protease (Q7K)	AQ148	−39.14	HOH402	ref 47
3DFR	dihydrofolate reductase	methotrexate	−58.76		ref 47
3PCK	protocatechuate 3,4-dioxygenase	6-hydroxynicotinic acid N-oxide	−38.22	Fe	ref 47
3YAS	hydroxynitrile lyase	acetone	−8.66		ref 21
4PHV	HIV-1 protease	L-700,417(R,R)	−52.34	HOH001	ref 21
4TIM	triosephosphate isomerase	2-phospho-glycerate	−12.32		ref 47
4TS1	tyrosyl-tRNA synthetase	tyrosine	−28.07		ref 41
5ABP	L-arabinose-binding protein	D-galactose	−37.88		ref 47
5CNA	concanavalin A	O1-methyl-mannose	−22.18	Ca	ref 35
6ABP	L-arabinose-binding protein (M108L)	L-arabinose	−36.26		ref 42
6APR	rhizopuspepsin	pepstatin	−44.33		ref 47
6RNT	ribonuclease T1	2-AMP	−13.52		ref 47
6TIM	triosephosphate isomerase	glycerol-3-phosphate	−18.31		ref 47
7ABP	L-arabinose-binding protein (M108L)	D-fucose	−31.61	HOH153	ref 47
7DFR	dihydrofolate reductase	folate	−28.30	NADPH	ref 11
7HVP	HIV-1 protease	JG-365	−54.88	HOH301	ref 43
7UPJ	HIV-1 protease	U101935	−48.44		ref 47
8ABP	L-arabinose-binding protein (M108L)	D-galactose	−45.64	HOH001	ref 47
9HVP	HIV-1 protease	A74704	−47.65	HOH001	ref 34

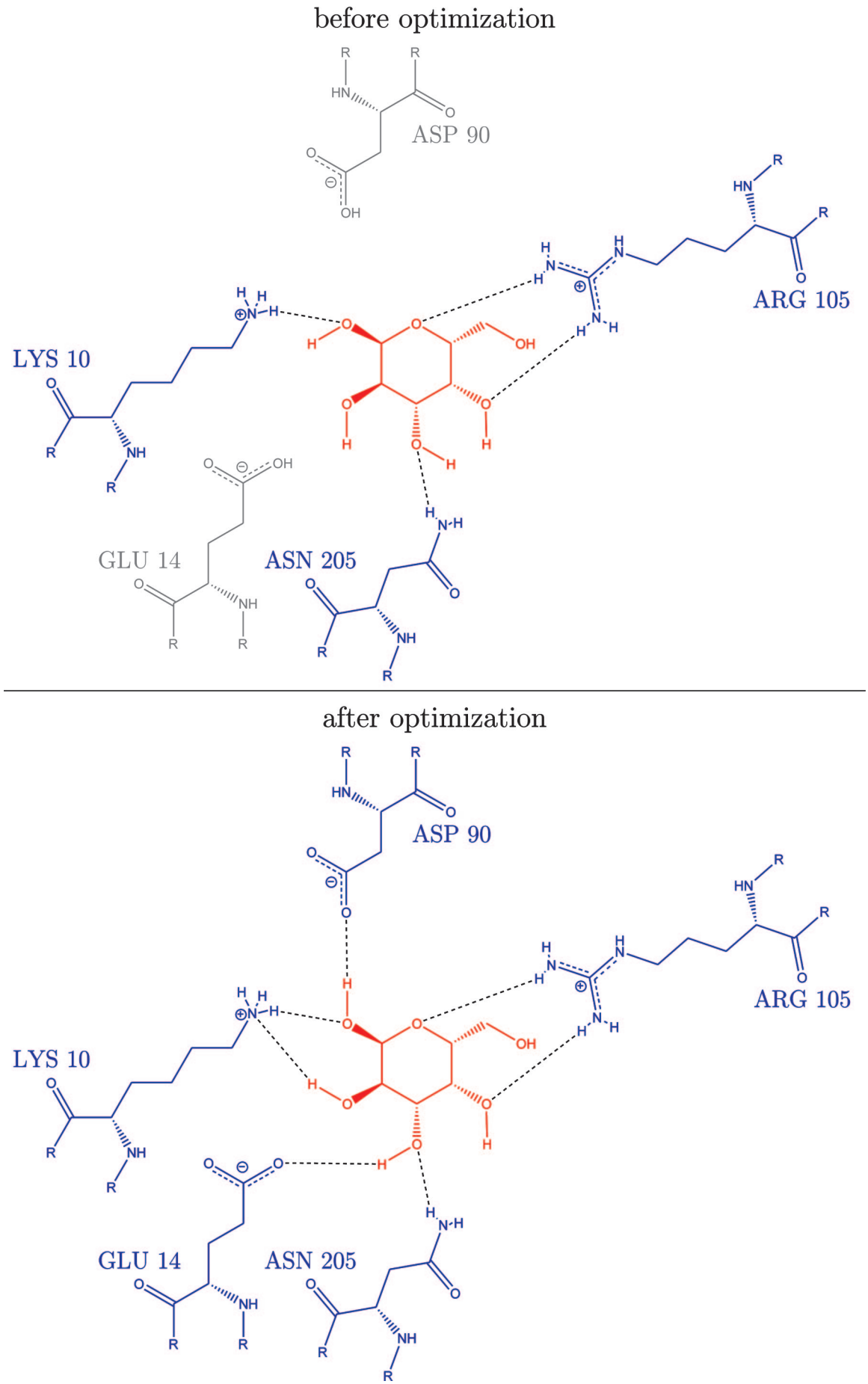

Figure 7. Complex 8ABP before and after the optimization of the dihedral angles of the hydrogen bond donors of the ligand.

N denotes the number of attractively scored complexes, these entities are defined by

$$R_P = \frac{\sum_i (x_i - \bar{x})(y_i - \bar{y})}{\sqrt{\sum_i (x_i - \bar{x})^2}\sqrt{\sum_i (y_i - \bar{y})^2}} \quad (6)$$

$$SD = \sqrt{\frac{\sum_i [y_i - (ax_i + b)]^2}{N - 2}} \quad (7)$$

$$ME = \frac{\sum_i |y_i - (ax_i + b)|}{N} \quad (8)$$

3. RESULTS AND DISCUSSION

3.1. Binding Energies. *3.1.1. AIScore.* The correlation plots in Figure 8 clearly show that AIScore with its chemically diverse increments and the XFurcate algorithm for handling multifurcated hydrogen bonds (Figure 8*a*) performs best in estimating the binding affinity of a protein−ligand complex in its experimental conformation. The Pearson linear correlation coefficient amounts to $R_P = 0.87$ ($r^2 = 0.76$) for the training set of 101 complexes, and the achieved RMSE is 6.76 kJ mol^{-1}.

Before analyzing a few apparent outliers, let us have a look at the optimized parameter set of AIScore (Table 3). From a chemical point of view it is noteworthy that the empirically optimized energy increments of charged hydrogen bond acceptors (sp^2 oxygen in carboxylate groups and phosphor acid esters) are so small, i.e., smaller than the increments of most of the neutral sp^2 oxygen hydrogen bond acceptors after scaling with f_s. The energy increments of protonated amines are even positive. Unless matched by a strongly negative acceptor increment, the energy increments of a salt bridge therefore add up to a positive ΔG_{ia} value. At first sight this result is counterintuitive, but the fit is robust in this respect. All attempts to guide the least-squares fit to a different minimum with negative energy increment for HN+(cmn) type interaction sites were unsuccessful. This result can be interpreted in two ways: (*i*) It is physically motivated. As stated in the literature,[61] the energetically favorable Coulombic charge−charge interaction is opposed by unfavorable desolvation of the interacting charges. In the context of protein folding, several cases were described where the net effect of a salt bridge was even destabilizing.[62] (*ii*) The scoring function is too crude, and the unexpectedly small or even positive values associated with the free energy increments of the ionic hydrogen bonds originate from the competition with other ΔG_{ia} contributions in the least-squares fit.

One major outlier is the complex 1CAQ which is the catalytic domain of the human stromelysin complexed with diphenyl piperidine sulfonamide ($\Delta G_{exp} = -44.40$ kJ mol^{-1}, AIScore = −67.39 kJ mol^{-1}). Of the 19 contacts which are formed by this complex, only two are hydrogen bonds: the nitrogen of the sulfonamide group forms a hydrogen bond with the peptide oxygen of ALA165, and one of the oxygens of the group forms a hydrogen bond with the peptide NH group of LEU164. In addition there is a metallic interaction between the group of the ligand and the zinc ion within the active site. The remaining 16 contacts are all multiple phenyl-CH contacts (see Figure 9). The individual match scores sum up to $\Delta G_{ia} = -15.52$ kJ mol^{-1}. A small positive contribution from atomic clashes $\Delta G_{clash} = 1.18$ kJ mol^{-1} and the constant shift of $G_0 = -5.74$ kJ mol^{-1} leaves an amount of −47.31 kJ mol^{-1} originating from $\Delta G_{lipo/ambig}$.

Another apparent outlier is the complex of dihydrofolate reductase and folate (7DFR, $\Delta G_{exp} = -28.30$ kJ mol^{-1}, AIScore = −45.10 kJ mol^{-1}). Again, most of the 15 occurring contacts are phenyl-CH contacts. Only three hydrogen bonds are formed between the ligand and the amino acids of the protein ASP27 and ARG57 (see Figure 10). The individual match scores sum up to $\Delta G_{ia} = -8.65$ kJ mol^{-1}. As in the previous case, the lipophilic interactions are severely overestimated.

Due to the predominance of lipohilic interactions in most of the protein−ligand complexes, it is clear that leaving out the XFurcate option for treating multifurcated bonds leads to minor deterioration of the general results. An example where multifurcated bonds play an important role is 2QWD. Two bifurcated H-bonds and one trifurcated H-bond are formed in this complex. The experimental ΔG value amounts to −28 kJ mol^{-1}. AIScore with XFurcate reproduces the free binding energy very well ($\Delta G = -29$ kJ mol^{-1}), without XFurcate the deviation is somewhat higher ($\Delta G = -33$ kJ mol^{-1}).

3.1.2. FlexXScore. Figure 8*c* shows the correlation between the experimental binding affinities and the original FlexX-Score. Only 94 of the 101 complexes exhibit negative free binding energies. The extremely low Pearson correlation coefficient of $R_P = 0.06$ ($RMSE = 24.86$ kJ mol^{-1}) reveals that no correlation exists in this case.

When applying the XFurcate algorithm (Figure 8*d*) in addition to FlexXScore, the linear correlation increases to a value of $R_P = 0.12$ ($RMSE = 25.38$ kJ mol^{-1}), but only 92 of the 101 protein−ligand complexes bind attractively.

Generally speaking, the main bulk of the binding energies estimated by FlexXScore only cover a small range between approximately $\Delta G = -30$ kJ mol^{-1} and $\Delta G = 0$ kJ mol^{-1} compared to the experimental binding energies ranging between $\Delta G = -60$ kJ mol^{-1} and $\Delta G = -8$ kJ mol^{-1}.

3.1.3. Optimized and Augmented FlexXScore. The optimization of the parameters in the original FlexXScore scheme with respect to binding affinities results in an increase of the Pearson correlation coefficient from $R_P = 0.06$ to $R_P = 0.64$ ($r^2 = 0.41$, $RMSE = 11.96$ kJ mol^{-1}) (Figure 8*e*). All 101 complexes are scored attractively. The XFurcate algorithm was not applied here. Among the extreme outliers are the complexes 1CAQ and 1BRA that were overscored by

Table 5. Assessment of Different Scoring Functions on the PDBbind Set[b]

scoring function	N	R_P	SD	ME
X-Score::HMScore[a]	800	0.57	1.82	1.42
DrugScore::Pair[a]	800	0.47	1.94	1.51
AIScore+XFurcate	799	0.46	1.96	1.54
AIScore	798	0.45	1.97	1.55
FlexXScore	739	0.17	2.18	1.75
FlexXScore+XFurcate	734	0.20	2.17	1.74
FlexXScore(opt)	799	0.43	1.99	1.55
FlexXScore(aug)	799	0.42	2.00	1.58

[a] From ref 59. [b] N is the number of complexes with positive binding scores, R_P is the Pearson correlation coefficient, SD is the standard deviation, and ME is the unsigned mean error.

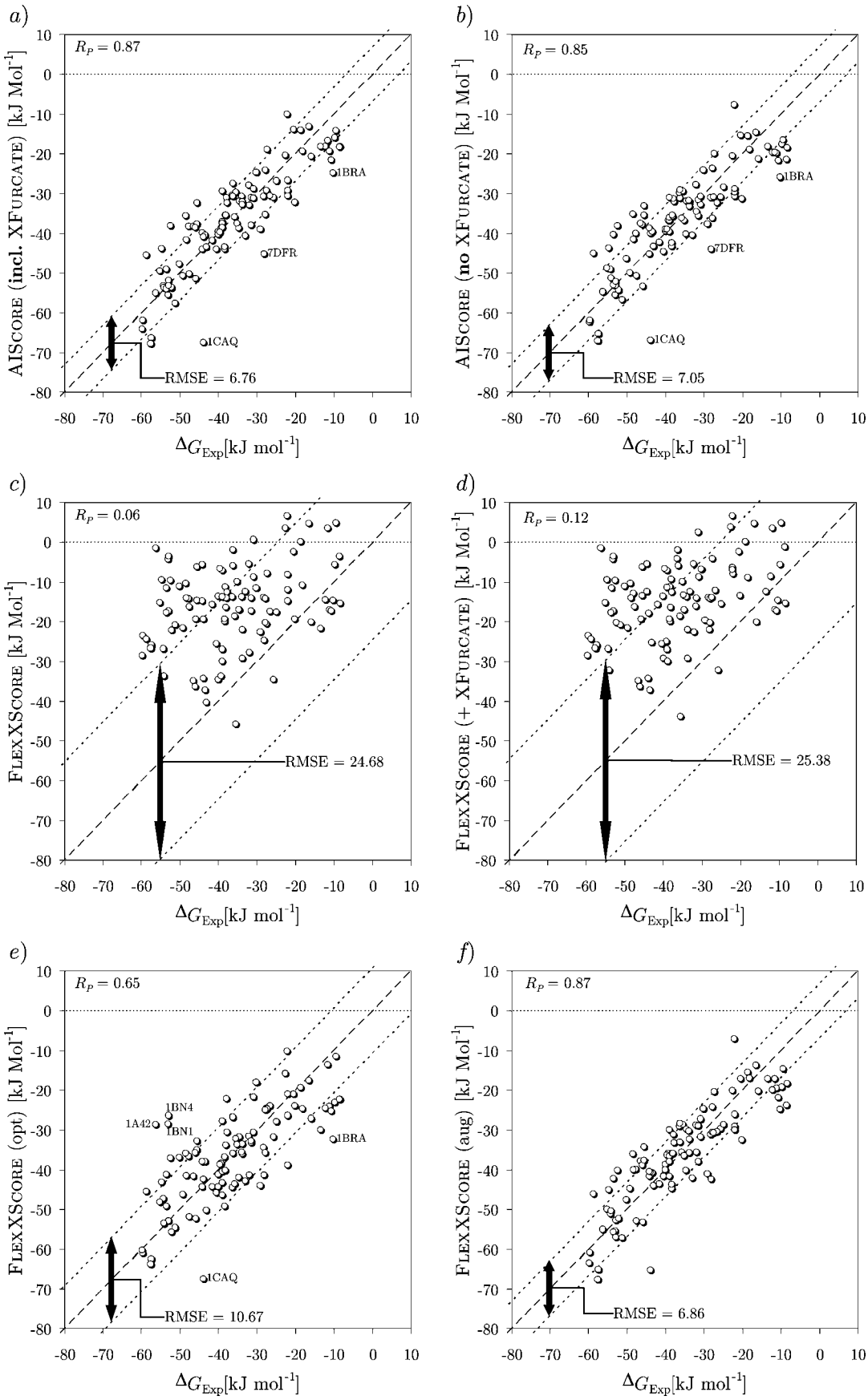

Figure 8. Linear correlations between the experimental free binding energy of the 101 complexes of the training set ΔG_{Exp} and the corresponding scored binding energy of the several scoring functions.

AIScore, too. On the other side, the complexes 1A42, 1BN4, and 1BN1 are substantially underscored by the FlexXScore-(opt), whereas AIScore matches nearly perfectly with experiment for these cases. The dominating binding motif in the latter three complexes is the interaction of negatively charged NH groups with an ion.

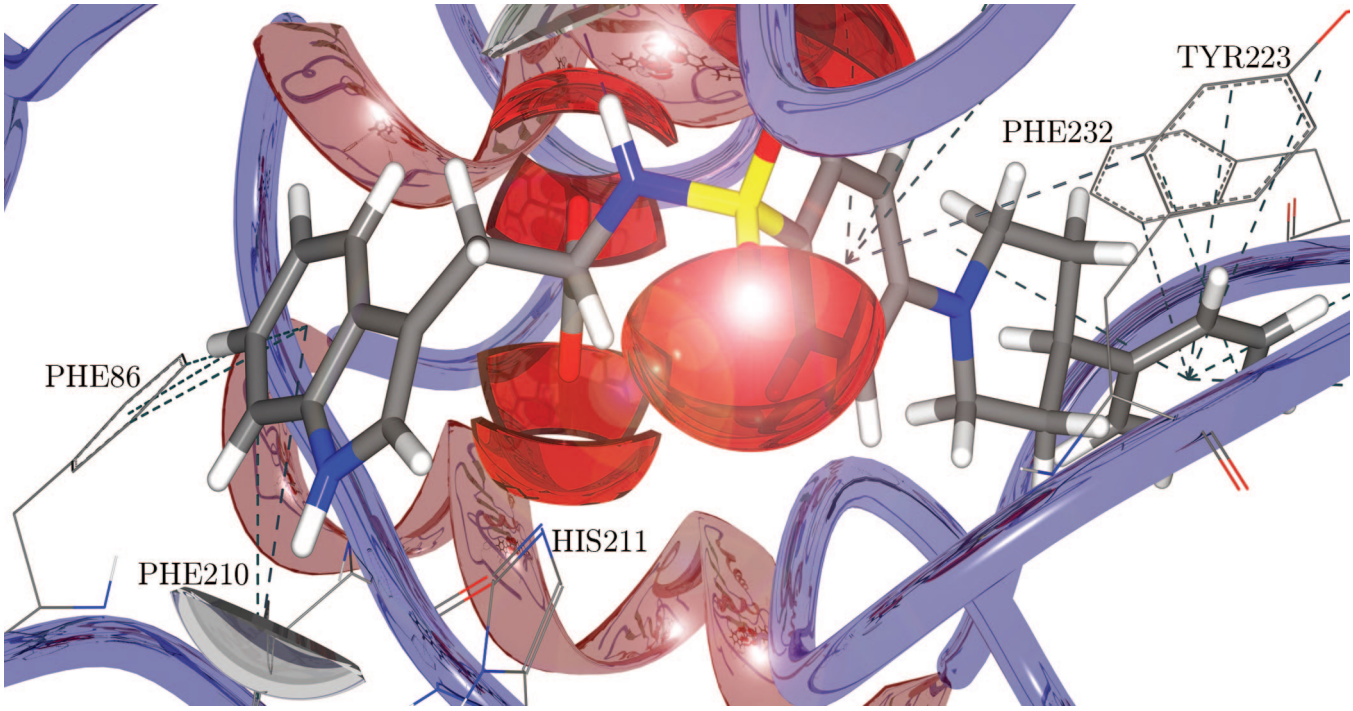

Figure 9. Complex 1CAQ with aromatic interactions (dotted lines).

The parameters of the FlexXScore(opt) scoring function are quite different from the original ones (see Table 1). For instance ΔG_0 changes from $\Delta G_0 = +5.4$ kJ mol^{-1} (original FlexXScore) to $\Delta G_0 = -10.59$ kJ mol^{-1} during the optimization. Also the $\Delta G_{lipo/ambig}$ terms of FlexXScore(opt) become strongly attractive.

FlexXScore(aug) shows an R_P of 0.87 ($r^2 = 0.75$) and an $RMSE = 6.86$ kJ mol^{-1} and thus performs as satisfactorily as AIScore in predicting the binding energies of the complexes of the training set. The good performance of FlexXScore(aug) in this respect is due to the large number of fit parameters rather than a good and realistic model. The subtle differences of these two scoring functions (individualized vs global increments for general neutral hydrogen bonds) become apparent in the validation procedures. AIScore shows substantially better results in predicting the binding energies of the PDBbind set and in rescoring given poses (see below).

The optimized parameters are shown in Table 3. It is seen that the increments of (partially) charged hydrogen bonds have even smaller absolute values than in the AIScore case. On the other hand, unrealistically large interaction increments for metallic interactions are found.

3.2. Validation. For assessing the performance of our scoring function we used the 800 entries of the "refined set" of the PDBbind database version 2002.[47,63] The proteins were used as provided by PDBbind. This ensures maximal compatibility with the above cited comparison studies of scoring functions. RDFWizard (see Section 2.3.2) was used to generate the required RDFs using the protonation state and hydroxyl/thiol torsion angles provided in PDBbind.

The success rates of the individual scoring functions in predicting the binding energies of the PDBbind test set are shown in Table 4 and compared with results of other scoring functions in the literature.[59] In these evaluation runs we strictly followed the protocol described in the original work. Wang et al.[59] divided the scoring functions into three classes: Those with Pearson correlation coefficients between $R_P = 0.57$ and $R_P = 0.45$ were considered to belong to the relatively successful ones, followed by a large group of middle-ranking scoring functions. The third group comprised those scoring functions which showed essentially no correlation with the experimental binding energies of the PDBbind set. The original FlexXScore belongs to the latter group.

For the assessment of the scoring functions optimized in this work it should be noted that 65 of the 800 complexes of the PDBbind test set were contained in our training set, whereas the training set of the most successful scoring function (X-Score::HMScore) and the PDBbind shared 140 data points.[59]

Plots of the linear correlations between the six scoring function addressed in this work (AIScore with and without XFurcate, FlexXScore with and without XFurcate, FlexXScore(opt), and FlexXScore(aug)) and the experimental binding energies of the PDBbind set are displayed in Figure 11.

Our tests confirm the results reported for FlexXScore in the literature.[59] Only 739 out of the 800 complexes are predicted to have attractive binding energies. The R_P value increases slightly from $R_P = 0.17$ to $R_P = 0.20$ when the XFurcate option is turned on, but both results must be considered unsatisfactory. The optimization of the 5 FlexXScore parameters with respect to the experimental binding energies of our training set dramatically improves the linear correlation with the PDBbind test set to $R_P = 0.43$ and promotes FlexXScore(opt) to the middle-ranking scoring functions. The number of unbound complexes has shrunk to 1 (1BJR).

To our great surprise, the success rate of the 15-parameter FlexXScore(aug) scoring function is a little lower than the one of the five-parameter FlexXScore(opt) function. The sheer number of parameters are therefore not the only reason for the good performance of AIScore in combination with XFurcate. With a Pearson correlation coefficient of $R_P = 0.46$ AIScore belongs to the group of relatively successful scoring functions as classified by Wang et al.[59] When comparing the success rates

of AIScore and the best scoring function from the literature (X-Score::HMScore, see Table 5) it should be noted, however, that unlike our training protocol (Figure 1) the PDBbind and the X-Score::HMScore training protocol[11] do not account for crystal water molecules. Therefore, protein−ligand complexes of the PDBbind test set, where essential water molecules mediate the interaction between protein and ligand, are systematically underrated by AIScore.

It has to be noted that until 2007 the original authors of PDBbind already discarded 142 of the 800 original entries of the 2002 version. The majority of these discarded entries are either "not valid" according to the definition in Wang et al.,[47] exhibit clashes, are covalently bound, or the respective binding affinity is either wrong or could not be confirmed (see the README.changes files of the PDBbind releases for more details). In several PDBbind entries IC_{50} values had been used instead of K_i values for the derivation of a binding energy.

3.3. Redocking. In order to test whether the optimization of the scoring functions with respect to binding affinities affects the docking capability of FlexX, we performed redocking experiments, i.e., for all of the 101 protein−ligand complexes we docked the ligand of the crystal structure back into its binding site. As performance criterion we used the root-mean-square deviation (RMSD) of the docked ligand conformation from the respective crystal structure

$$RMSD = \sqrt{\frac{\sum_i^n (x_{docked}(i) - x_{crystal}(i))^2}{n}} \quad (9)$$

where the sum runs over all n non-hydrogen atoms of the ligand. In Figure 12, the cumulative share of complexes is plotted against the corresponding RMSD for three scenarios. On the left (Figure 12*a*), only the best 20 ranked poses are taken into account. The right-hand plot (Figure 12*b*) displays the RMSD of the best pose independent of its rank. In the third scenario (Figure 12*c*) the reference structure was added before ranking since it is not generally guaranteed that a near-native pose is among all generated poses. We performed the redocking experiment with FlexXScore and AIScore each with and without the XFurcate algorithm. Additionally, we used the optimized and the augmented version of FlexXScore without the XFurcate algorithm for a redocking run.

As the number of conformations of a ligand increases exponentially with the number of freely rotatable bonds, the conformational space is searched by a k-greedy mechanism in FlexX.[12] The poses are generated according to the incremental construction scheme. Herein, base fragments of the chemical structure and the orientations of additional increments are selected according to energy criteria. For all scoring functions the same energy selection thresholds as in the original FlexXScore were employed.

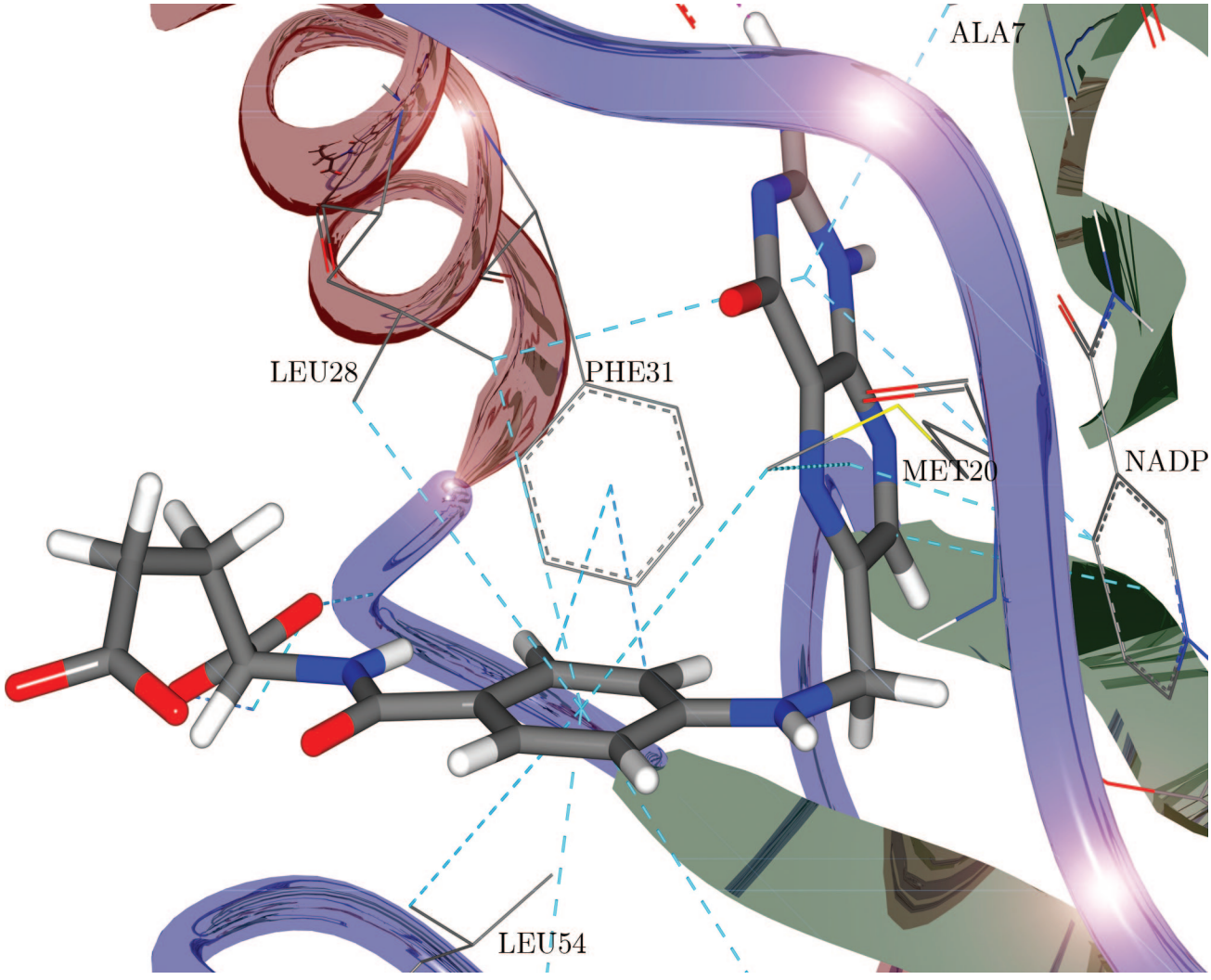

Figure 10. Complex 7DFR with aromatic interactions (dotted lines).

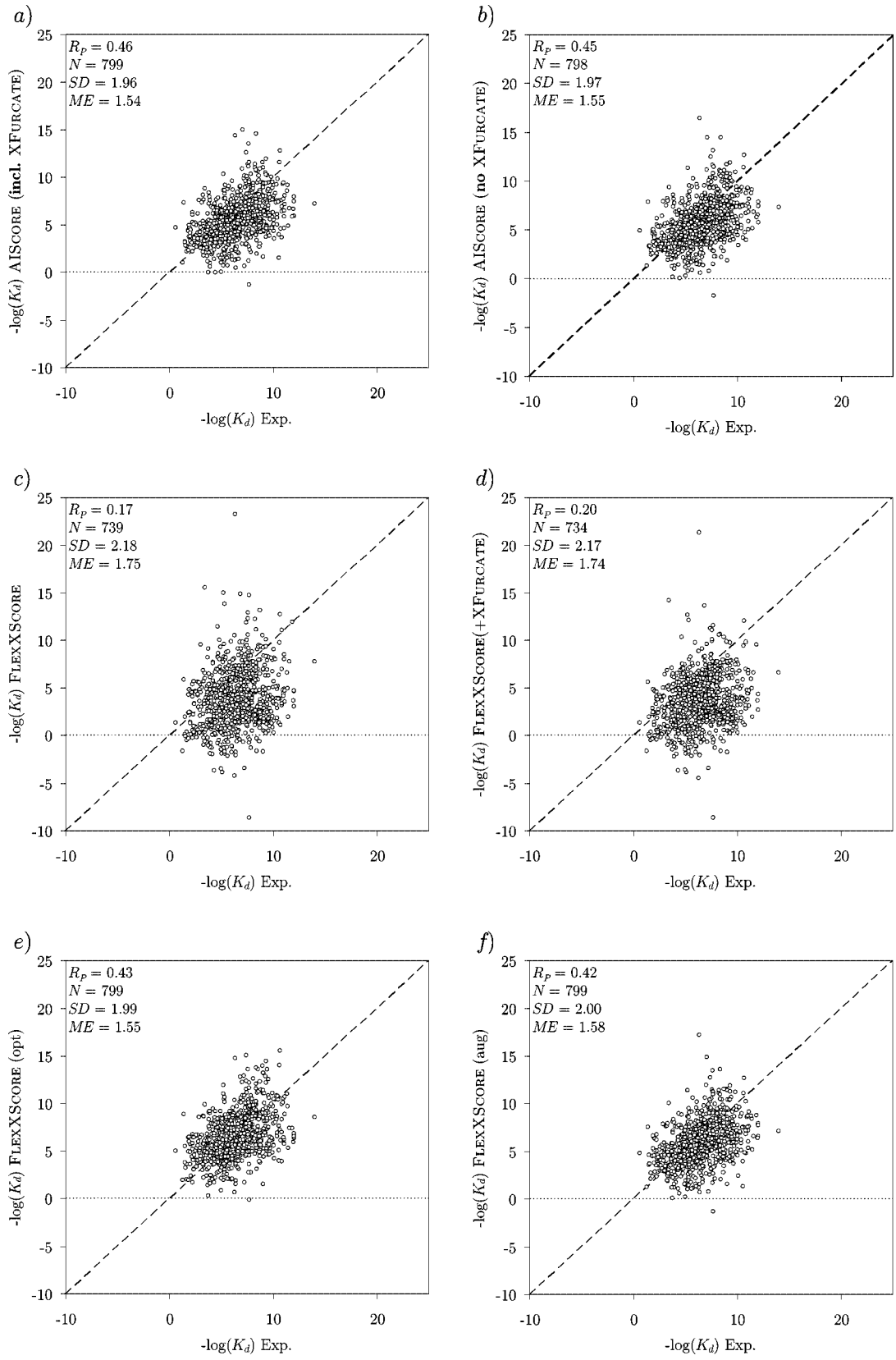

Figure 11. Linear correlations between the experimental and the scored pK values of the several scoring functions for the PDBbind.

To judge the global performance of FlexX in this respect it should be mentioned that some of the proteins, such as the HIV-1 proteases, are C_2-symmetric. The same is true for some ligands. We have not checked the highest ranked solutions of a docking run for symmetry equivalences. A large RMSD may therefore simply result from an interchange of symmetry equivalent atoms.

The first two scenarios (Figure 12*a*,*b*) give similar results. Of all scoring functions the original FlexXScore performs best in the redocking experiment. If the threshold for a valid

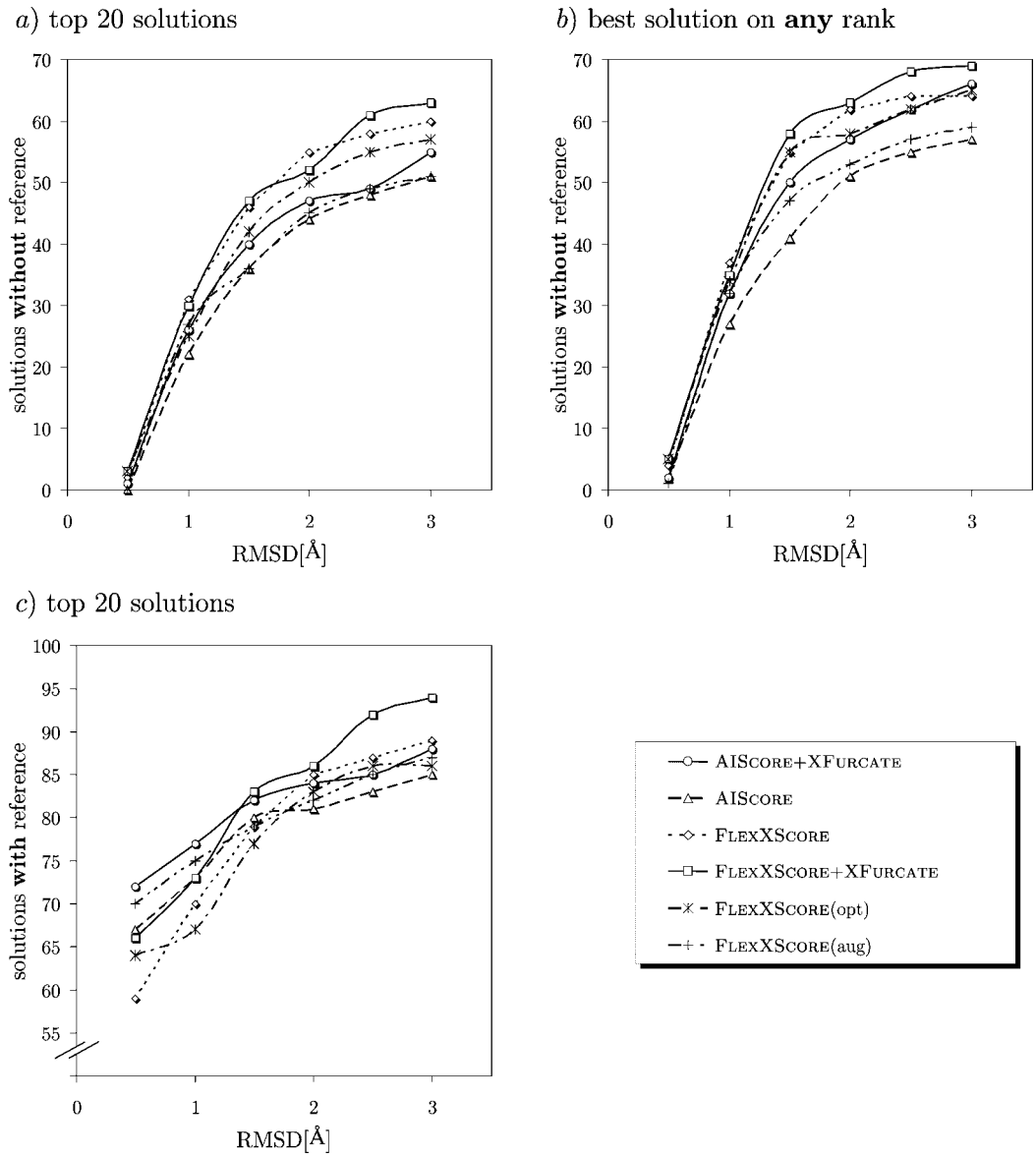

Figure 12. Comparison of the cumulative shares of complexes against the corresponding RMSD.

solution is set to 2 Å, FlexXScore succeeds in 55 out of the 101 cases. However, the resolution of the experimental structures is closer to 2.5 Å in most complexes. Therefore it appears to be more meaningful to set the threshold to the latter value. In this case, the cumulative success rate is increased to 58 and is improved further to 61 if the XFurcate algorithm is applied. The redocking capabilities of AIScore with or without XFurcate are significantly lower. FlexXScore(opt) ranges in between whereas FlexXScore(aug) performs similarly to AIScore without XFurcate. It thus appears that the redocking capability deteriorates with improved binding affinity prediction. With regard to timings, redocking runs employing AIScore are only marginally (4%) slower than the corresponding runs utilizing FlexXScore.

In the third scenario, where the reference structure was added to the pool of all generated complex geometries *a posteriori*, a more subtle picture emerges. For RMSD values of 1.0 Å and below, i.e., the range where it is essential to identify the reference structure among all placements solely on the basis of its energy, AIScore with XFurcate is superior to the other five scoring functions. At larger RMSD values, the picture observed already in the first scenario is restored. We interpret these results as follows. When AIScore is used in the incremental build-up of the chemical structure of the ligand, fewer near-native posings are generated than for FlexXScore. Thus, despite its higher capability of recognizing an energetically favorable structure, AIScore shows an inferior docking performance. XFurcate improves the success rate in both cases.

An obvious reason, why the geometries of the poses generated with AIScore are less reliable than for FlexXScore, is the loss of directional forces in the case of salt bridges. Due to their small (or even repulsive) increments in the AIScore scoring function their energy contributions to the differential free energy are easily outweighed by nondirectional contact terms. The same is true for FlexXScore(aug) and to a lesser extent for FlexXScore(opt).

Furthermore, in FlexX the score of the remaining, i.e., still to be incrementally constructed fragments, is estimated using the maximal energy these fragments can contribute. So far, this estimation does not take the individual increments of AIScore into account and, thus, cannot give a reliable estimation of the remaining energy. This is another reason

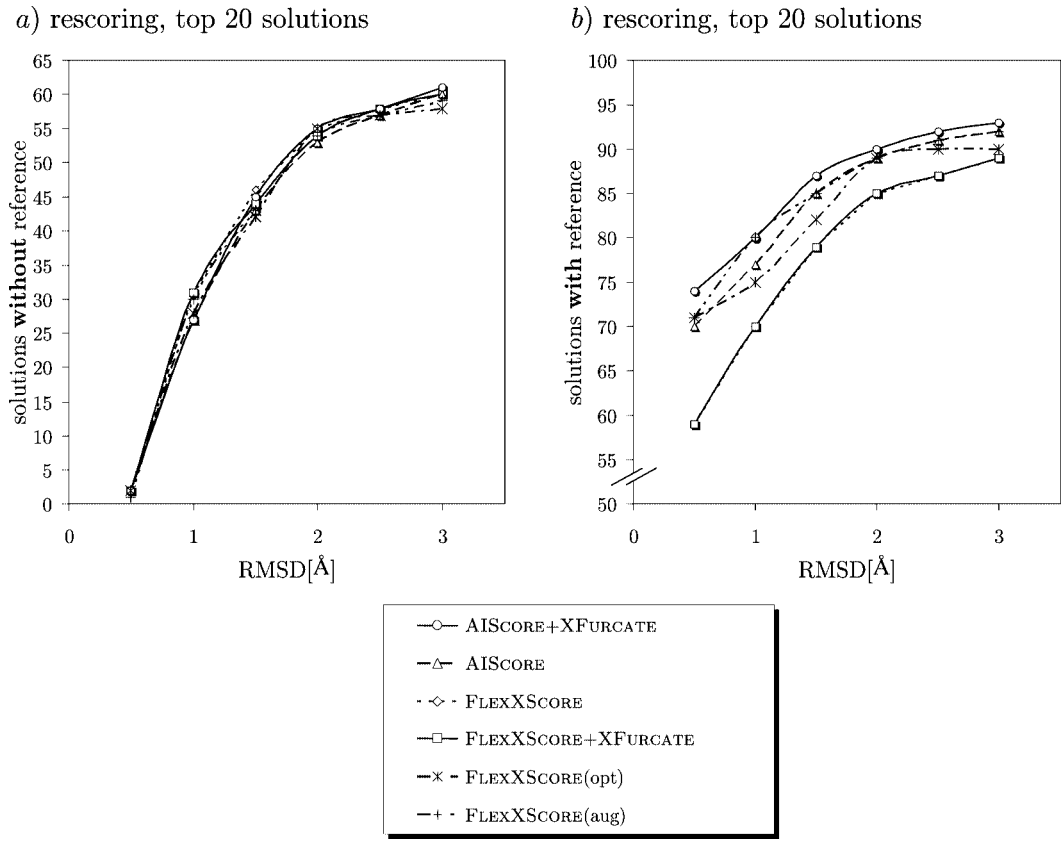

Figure 13. Comparison of the rescoring performance of various scoring functions.

why AIScore should not be used during incremental construction.

3.4. Rescoring. As can be seen in Section 3.3, redocking is quite sensitive to the utilized scoring function. To evaluate the capability of the particular scoring functions under equivalent conditions, we applied the following rescoring protocol. First we employed the original FlexXScore with the default docking parameters to redock the 101 complexes. We stored all generated poses for each complex. Subsequently, we rescored all poses of a complex with the remaining five scoring functions and reranked them on the basis of their new scores. Finally, we carried out the same RMSD analysis as described before. This rescoring protocol ensures that all scoring functions need to identify the near-native pose out of the same pool of decoys.

Different results are obtained depending on the question whether the reference structure was added to the generated poses before reranking or not. Let us first consider the top 20 solutions of the rescoring process without explicit addition of the reference (Figure 13*a*). In this case all scoring functions yield roughly the same results. If it is guaranteed that the reference structure is present among the generated poses, the picture changes (Figure 13*b*). Setting the threshold for a valid structure again to an RMSD value of 2.5 Å, AIScore shows a success rate of better than 90% in combination with XFurcate. The other scoring functions which were reparameterized to fit the binding affinities of the training set perform only slightly less optimal. In this setup FlexXScore shows a somewhat reduced performance.

4. CONCLUSION

By introducing chemically diverse hydrogen binding energies, a significant improvement in the description of protein−ligand binding affinities has been achieved compared to the original FlexX scoring function FlexXScore. In total 15 parameters were fitted to experimental binding affinities of 101 protein−ligand complexes. Among these are the energy increments of lipophilic and metallic interactions as well as a few types of ionic or resonance-enhanced hydrogen bonds, while most of the hydrogen bond strengths were derived from the results of quantum chemical *ab initio* calculations *in vacuo*. A single scaling factor for the *ab initio* energy increments of hydrogen bond donors and acceptors proved to be sufficient to account for solvation effects. From validation calculations on the PDBbind test set comprising 800 protein−ligand complexes with experimentally known affinities, we deduce that the good performance of our novel scoring function AIScore is not a result of overtraining on our data set.

All results presented here were obtained for experimental complex geometries. First tests where AIScore has been employed in flexible docking studies instead of FlexXScore indicate that the well-known efficiency of FlexX in predicting the geometric position of a ligand in the protein binding pocket is not fully reached. How this problem can be tackled, will be addressed in future work. At the present stage, it may therefore be advised to use FlexXScore during the incremental construction phase and then rescore the poses with AIScore to obtain a good estimate of the binding affinity.

For the scoring of multifurcated hydrogen bonds, the XFurcate scheme was devised where each hydrogen bond donor or acceptor contributes its match score only once. XFurcate improves the binding affinities as well as the redocking capabilities of both, AIScore and the original

FlexXScore. It is therefore recommended to use the XFurcate scheme throughout.

ACKNOWLEDGMENT

The authors are grateful to J. Apostolakis (LMU München), J. Rahnenführer and T. Lengauer (MPI Informatik, Saarbrücken), M. Gastreich (BioSolveIT, St. Augustin), and M. Rarey (ZBH Hamburg) for valuable discussions. S.R. and C.M.M. would like to express their thanks to BioSolveIT (St. Augustin) for a free developer version of the FlexX software. This work was supported by Deutsche Forschungsgemeinschaft through projects MA 1051/6 and KA 1804/1.

Supporting Information Available: Subgraph trees of hydrogen bond donors and acceptors employed in AIScore. This material is available free of charge via the Internet at http://pubs.acs.org.

REFERENCES AND NOTES

(1) Ewing, T. J.; Makino, S.; Skillman, A. G.; Kuntz, I. DOCK 4.0: Search Strategies for Automated Molecular Docking of Flexible Molecule Databases. *J. Comput.-Aided Mol. Des.* **2001**, *15*, 411–428.
(2) Klebe, G. Virtual Ligand Screening: Strategies, Perspectives and Limitations. *Drug Discovery Today* **2006**, *11*, 580–594.
(3) Rarey, M.; Lengauer, T.; Klebe, G. A Fast Flexible Docking Method Using an Incremental Construction Algorithm. *J. Mol. Biol.* **1996**, *261*, 470–489.
(4) Jones, G.; Willet, P.; Glenn, R. C.; Leach, A. R.; Taylor, R. Developement and Validation of a Genetic Algorithm for Flexible Docking. *J. Mol. Biol.* **1997**, *267*, 727–748.
(5) Morris, G. M.; Goodsell, D. S.; Halliday, R. S.; Huey, R.; Hart, W. E.; Belew, R. K.; Olson, A. J. Automated Docking Using a Lamarckian Genetic Algorithm and an Empirical Binding Free Energy Function. *J. Comput. Chem.* **1998**, *19*, 1639–1662.
(6) Friesner, R. A.; Banks, J. L.; Murphy, R.; Halgren, T. A.; Klicic, J. J.; Mainz, D. T.; Repasky, M. P.; Knoll, E. H.; Shelley, M.; Perry, J. K.; Shaw, D. E.; Francis, P.; Shenkin, P. S. GLIDE: A New Approach for Rapid, Accurate Docking and Scoring. 1: Method and Assessment of Docking Accuracy. *J. Med. Chem.* **2004**, *47*, 1739–1749.
(7) Owens, J.; Lipinski, C. Chris Lipinski Discusses Life and Chemistry After the Rule of Five. *Drug Discovery Today* **2003**, *8*, 12–16.
(8) Velec, H. F.; Gohlke, H.; Klebe, G. DrugScore^{CSD} -- Knowledge-Based Scoring Function Derived from Small Molecule Crystal Data With Superior Recognition Rate of Near-Native Ligand Poses and Better Affinity Prediction. *J. Med. Chem.* **2005**, *48*, 6296–6303.
(9) Gohlke, H.; Klebe, G. Approaches to the Description and Prediction of the Binding Affinity of Small-Molecule Ligands to Macromolecular Receptors. *Angew. Chem., Int. Ed.* **2002**, *41*, 2645–2676.
(10) Böhm, H. J. The Development of a Simple Empirical Scoring Function To Estimate the Binding Constant for a Protein Ligand Complex of Known 3-Dimensional Structure. *J. Comput.-Aided Mol. Des.* **1994**, *8*, 243–256.
(11) Wang, R. X.; Liu, L.; Lai, L. H.; Tang, Y. Q. SCORE: A New Empirical Method for Estimating the Binding Affinity of a Protein-Ligand Complex. *J. Mol. Model.* **1998**, *4*, 379–394.
(12) Kramer, B.; Rarey, M.; Lengauer, T. Evaluation of the FlexX Incremental Construction Algorithm for Protein-Ligand Docking. *Proteins: Struct., Funct., Genet.* **1999**, *37*, 228–241.
(13) Eldridge, M. D.; Murray, M. D.; Auton, T. R.; Paolini, G. W.; Mee, R. P. Empirical Scoring Functions. I. The Development of a Fast Empirical Scoring Function to Estimate the Binding Affinity of Ligands in Receptor Complexes. *J. Comput.-Aided Mol. Des.* **1997**, *11*, 425–445.
(14) Huang, S. Y.; Zou, X. Q. An Iterative Knowledge-Based Scoring Function to Predict Protein-Ligand Interactions: I. Derivation of Interaction Potentials. *J. Comput. Chem.* **2006**, *27*, 1866–1875.
(15) Gohlke, H.; Hendlich, M.; Klebe, G. Knowledge-Based Scoring Function to Predict Protein-Ligand Interactions. *J. Mol. Biol.* **2000**, *295*, 337–356.
(16) Muegge, I.; Martin, Y. C. A General and Fast Scoring Function for Protein-Ligand Interactions: A Simplified Potential Approach. *J. Med. Chem.* **1999**, *42*, 791–804.
(17) Mitchell, J. B. O.; Laskowski, R. A.; Thornton, A. A. J. M. BLEEP - Potential of Mean Force Describing Protein-Ligand Interactions: I. Generating Potential. *J. Comput. Chem.* **1999**, *20*, 1165–1176.
(18) Gelin, B. R.; Karplus, M. Side-Chain Torsional Potentials -- Effect of Dipeptide, Protein, and Solvent Environment. *Biochemistry* **1979**, *18*, 1256.
(19) Brooks, B. R.; Bruccoleri, R. E.; Olafson, B. B.; States, D. J.; Swaminathan, S.; Karplus, M. CHARMM: A Program for Macromolecular Energy, Minmimization, and Dynamics Calculations. *J. Comput. Chem.* **1983**, *4*, 187.
(20) Cornell, W. D.; Cieplak, P.; Bayly, C. I.; Gould, I. R.; Merz, K. M., Jr.; Ferguson, D. M.; Spellmeyer, D. C.; Fox, T.; Caldwell, J. W.; A., P.; Kollman, A. Second Generation Force Field for the Simulation of Proteins, Nucleic Acids and Organic Molecules. *J. Am. Chem. Soc.* **1995**, *117*, 5179–5197.
(21) Raha, K., Jr. Large-Scale Validation of a Quantum Mechanics Based Scoring Function: Predicting the Binding Affinity and the Binding Mode of a Diverse Set of Protein-Ligand Complexes. *J. Med. Chem.* **2005**, *48*, 4558–4575.
(22) Raub, S.; Marian, C. M. Quantum Chemical Investigation of Hydrogen-Bond Strengths and Partition into Donor and Acceptor Contributions. *J. Comput. Chem.* **2007**, *28*, 1503–1515.
(23) Böhm, H. J. LUDI - Rule-Based Automatic Design of New Substituents for Enzyme-Inhibitor Leads. *J. Comput.-Aided Mol. Des.* **1992**, *6*, 593–606.
(24) Klebe, G. The Use of Composite Crystal-Field Environments in Molecular Recognition and the De-Novo Design of Protein Ligands. *J. Mol. Biol.* **1994**, *237*, 221–235.
(25) Berman, H. M.; Westbrook, J.; Feng, Z.; Gililand, G.; Baht, T. N.; Weissig, H.; Shindyalov, I. N.; Bourne, P. E. The PDBbind Database: Collection of Binding Affinities for Protein-Ligand Complexes with Known Three-Dimensional Structures. *Nucleic Acids Res.* **2000**, *28*, 235–242.
(26) Tsuzuki, S.; Lüthi, H. P. Effects of Basis Set and Electron Correlation on the Calculated Interaction Energies of Hydrogen Bonding Complexes: MP2/cc-pV5Z Calculations of H2O-MeOH, H2O-Me2O, H2O-H2CO, MeOH-MeOH, and HCOOH-HCOOH Complexes. *J. Chem. Phys.* **2001**, *114*, 3949–3957.
(27) Huang, N.; MacKerell, A. D., Jr. An Ab Initio Quantum Mechanical Study of Hydrogen-Bonded Complexes of Biological Interest. *J. Phys. Chem. A* **2002**, *106*, 7820–7827.
(28) Sponer, J.; Jurecka, P.; Hobza, P. Accurate Interaction Energies of Hydrogen-Bonded Nucleic Acid Base Pairs. *J. Am. Chem. Soc.* **2004**, *126*, 10142–10151.
(29) Albrecht, G.; Corey, R. B. The Crystal Structure of Glycine. *J. Am. Chem. Soc.* **1939**, *61*, 1087.
(30) Rozas, I.; Alkorta, I.; Elguero, J. Bifurcated Hydrogen Bonds: Three-Centered Interactions. *J. Phys. Chem.* **1998**, *102*, 9925–9932.
(31) Rupp, B.; Raub, S.; Marian, C.; Höltje, H. D. Molecular Design of Two Sterol 14-α-Demethylase Homology Models and Their Interactions with the Azole Antifungals Ketoconazole and Bifonazole. *J. Comput.-Aided Mol. Des.* **2005**, *19*, 149–163.
(32) Schöneboom, J. C.; Lin, H.; Reuter, N.; Thiel, W.; Cohen, S.; Ogliaro, F.; Shaik, S. The Elusive Oxidant Species of Cytochrome P450 Enzymes: Characterization by Combined Quantum Mechanical/Molecular Mechanical QM/MM Calculations. *J. Am. Chem. Soc.* **2002**, *124*, 8142–8151.
(33) Borowski, T.; Siegbahn, P. E. M. Modeling Enzymatic Reactions Involving Transition Metals. *Acc. Chem. Res.* **2006**, *39*, 729–738.
(34) Wang, R.; Lai, L.; Wang, S. Further Development and Validation of Empirical Scoring Functions for Structure-Based Binding Affinity Prediction. *J. Comput.-Aided Mol. Des.* **2002**, *16*, 11–26.
(35) Kerzmann, A.; Neumann, D.; Kohlbacher, O. SLICK - Scoring and Energy Functions for Protein-Carbohydrate Interactions. *J. Chem. Inf. Model.* **2006**, *46*, 1635–1642.
(36) Böhm, H. J. Prediction of Binding Constants of Protein Ligands: A Fast Method for the Prioritization of Hits Obtained from De Novo Design or 3D Database Search Programs. *J. Comput.-Aided Mol. Des.* **1998**, *12*, 309–323.
(37) Wedemayer, G. J.; Patten, P. A.; Wang, L. H.; Schultz, P. G.; Stevens, R. C. Structural Insights into the Evolution of an Antibody Combining Site. *Science* **1997**, *276*, 1665–1669.
(38) McMillan, K.; Adler, M.; Auld, D. S.; Baldwin, J. J.; Blasko, E.; Browne, L. J.; Chelsky, D.; Davey, D.; Dolle, R. E.; Eagen, K. E.; Erickson, S.; Feldman, R. I.; Glaser, C. B.; Mallari, C.; Morrissey, M. M.; Ohlmeyer, M. H. J.; Pan, G.; Parkinson, J. F.; Phillips, G. B.; Polokoff, M. A.; Sigal, N. H.; Vergona, R.; Whitlow, M.; Young, T. A.; Devlin, J. J. Allosteric Inhibitors of Inducible Nitric Oxide Synthase Dimerization Discovered via Combinatorial Chemistry. *Proc. Natl. Acad. Sci. U.S.A.* **2000**, *97*, 1506–1511.
(39) Hosur, M. V.; Bhat, T. N.; Kempf, D. J.; Baldwin, E. T.; Liu, B. S.; Gulnik, S.; Wideburg, N. E.; Norbeck, D. W.; Appelt, K.; Erickson, J. W. Influence of Stereochemistry on Activity and Binding Modes for C(2) Symmetry-Based Diol Inhibitors of HIV-1 Protease. *J. Am. Chem. Soc.* **1994**, *116*, 847–855.

(40) Turk, D.; Stürzebecher, J.; Bode, W. Geometry of Binding of the N Alpha-Tosylated Piperidides of m-Amidino-, p-Amidino- and p-Guanidino Phenylalanine to Thrombin and Trypsin. X-Ray Crystal Structures of their Trypsin Complexes and Modeling of their Thrombin Complexes. *FEBS Lett.* **1991**, *287*, 133–138.
(41) Wells, T. N.; Fersht, A. R. Use of Binding Energy in Catalysis Analyzed By Mutagenesis of the Tyrosyl-tRNA Synthetase. *Biochemistry* **1986**, *25*, 1881–1886.
(42) Vermersch, P. S.; Lemon, D. D.; Tesmer, J. J.; Quiocho, F. A. Sugar-Binding and Crystallographic Studies of an Arabinose-Binding Protein Mutant (Met108Leu) that Exhibits Enhanced Affinity and Altered Specificity. *Biochemistry* **1991**, *30*, 6861–6866.
(43) Swain, A. L.; Miller, M. M.; Green, J.; Rich, D. H.; Schneider, J.; Kent, S. B.; Wlodawer, A. X-Ray Crystallographic Structure of a Complex Between a Synthetic Protease of Human Immunodeficiency Virus 1 and a Substrate-Based Hydroxyethylamine Inhibitor. *Proc. Natl. Acad. Sci. U.S.A.* **199**, *87*, 8805–8809.
(44) Boriack-Sjodin, P. A.; Zeitlin, S.; Chen, H. H.; Crenshaw, L.; Gross, S.; Dantanarayana, A.; Delgado, P.; May, J. A.; Dean, T.; Christianson, D. W. Structural Analysis of Inhibitor Binding to Human Carbonic Anhydrase II. *Protein Sci.* **1998**, *7*, 2483–2489.
(45) Brown, M.; Schumacher, M. A.; Wiens, G. D.; Brennan, R. G.; Rittenberg, M. B. The Structural Basis of Repertoire Shift in an Immune Response to Phosphocholine. *J. Exp. Med.* **2000**, *191*, 2101–2112.
(46) Vega, S.; Kang, L. W.; Velazquez-Campoy, A.; Kiso, Y.; Amzel, L. M.; Freire, E. A Structural and Thermodynamic Escape Mechanism from a Drug Resistant Mutation of the HIV-1 Protease. *Proteins: Struct., Funct., Genet.* **2004**, *55*, 594–602.
(47) Wang, R. X.; Fang, X. L.; Lu, Y. P.; Wang, S. M. The PDBbind Database: Collection of Binding Affinities for Protein-Ligand Complexes with Known Three-Dimensional Structures. *J. Med. Chem.* **2004**, *47*, 2977–2980.
(48) Word, J. M.; Lovell, S. C.; Richardson, J. S.; Richardson, D. C. Asparagine and Glutamine: Using Hydrogen Atom Contacts in the Choice of Side-Chain Amide Orientation. *J. Mol. Biol.* **1999**, *285*, 1735–1747.
(49) Levitt, M.; Park, B. H. Water - Now You See It, Now You Don't. *Structure* **1993**, *1*, 223–226.
(50) Carugo, O.; Bordo, D. How Many Water Molecules Can Be Detected by Protein Crystallography. *Acta Crystallogr., Sect. D* **1999**, *55*, 479–483.
(51) Garcia-Sosa, A. T.; Mancera, R. L.; Dean, P. M. WaterScore: A Novel Method for Distinguishing Between Bound and Displaceable Water Molecules in the Crystal Structure of the Binding Site of Protein-Ligand Complexes. *J. Mol. Model.* **2003**, *9*, 172–182.
(52) Giacovazzo, C.; Monaco, H. L.; Artioli, G.; Viterbo, D.; Ferraris, G.; Gilli, G.; Zanotti, G.; Catti, M. Fundamentals of Crystallography. *Fundamentals of Crystallography*; Oxford, 1992.
(53) McPhalen, C. A.; James, M. N. G. Structural Comparison of 2 Serine Proteinase Protein Inhibitor Complexes -- Eeglin-C-Subtilisin Carlsberg and CI-2-Subtilisin Novo. *Biochemistry* **1988**, *27*, 6582–6598.
(54) Halgren, T. A. Merck Molecular Force Field. II. MMFF94 van der Waals and Electrostatic Parameters for Intermolecular Interactions. *J. Comput. Chem.* **1996**, *17*, 520–552.
(55) Sadowski, J.; Gasteiger, J. From Atoms and Bonds to Three-Dimensional Atomic Coordinates: Automatic Model Builders. *Chem. Rev.* **1993**, *93*, 2567–2581.
(56) Kämper, A.; Apostolakis, J.; Rarey, M.; Marian, C. M.; Lengauer, T. Fully Automated Flexible Docking of Ligands into Flexible Synthetic Receptors Using Forward and Inverse Docking Strategies. *J. Chem. Inf. Model.* **2006**, *46*, 903–911.
(57) Steffen, A.; Kämper, A.; Lengauer, T. Flexible Docking of Ligands into Synthetic Receptors Using a Two-Sided Incremental Construction Algorithm. *J. Chem. Inf. Model.* **2006**, *46*, 1695–1703.
(58) Clark, M.; Cramer, R. D., III; van Opdenbosch, N. Validation of the General Purpose Tripos 5.2 Force Field. *J. Comput. Chem.* **1989**, *10*, 982–1012.
(59) Wang, R. X.; Lu, Y. P.; Fang, X.; Wang, S. M. An Extensive Test of 14 Scoring Functions Using the PDBbind Refined Set of 800 Protein–Ligand Complexes. *J. Chem. Inf. Model.* **2004**, *44*, 2114–2125.
(60) Huang, S. Y.; Zou, X. Q. An Iterative Knowledge-Based Scoring Function to Predict Protein-Ligand Interactions: II. Validation of the Scoring Function. *J. Comput. Chem.* **2006**, *27*, 1876–1882.
(61) Bossard, H. R.; Marti, D. N; Jelesarov, I. Protein Stabilization by Salt Bridges: Concepts, Experimental Approaches and Clarification of Some Misunderstandings. *J. Mol. Recognit.* **2004**, *17*, 1–16.
(62) Hendsch, Z. S.; Tidor, B. Do Salt Bridges Stabilize Proteins? A Continuum Electrostatic Analysis. *Protein Sci.* **1994**, *3*, 211–226.
(63) Wang, R. X.; Fang, X. L.; Lu, Y. P.; Wang, S. M. The PDBbind Database: Methodologies and Updates. *J. Med. Chem.* **2005**, *48*, 4111–4119.

CI7004669